

Myosin1G promotes Nodal signaling to control zebrafish left-right asymmetry

Received: 3 September 2023

Accepted: 22 July 2024

Published online: 02 August 2024

 Check for updatesAkshai Janardhana Kurup¹, Florian Bailet¹ & Maximilian Fürthauer¹  

Myosin1D (Myo1D) has recently emerged as a conserved regulator of animal Left-Right (LR) asymmetry that governs the morphogenesis of the vertebrate central LR Organizer (LRO). In addition to Myo1D, the zebrafish genome encodes the closely related Myo1G. Here we show that while Myo1G also controls LR asymmetry, it does so through an entirely different mechanism. Myo1G promotes the Nodal-mediated transfer of laterality information from the LRO to target tissues. At the cellular level, Myo1G is associated with endosomes positive for the TGF β signaling adapter SARA. *myo1g* mutants have fewer SARA-positive Activin receptor endosomes and a reduced responsiveness to Nodal ligands that results in a delay of left-sided Nodal propagation and tissue-specific laterality defects in organs that are most distant from the LRO. Additionally, Myo1G promotes signaling by different Nodal ligands in specific biological contexts. Our findings therefore identify Myo1G as a context-dependent regulator of the Nodal signaling pathway.


Left-Right (LR) asymmetries in the positioning and shape of different tissues are found in both protostome and deuterostome lineages and are critically required for human organ function¹. In spite of the importance of LR asymmetry, our understanding of the mechanisms that govern this third body axis remains fragmentary. A particularly striking feature of LR asymmetry is the fact that an evolutionary conserved mechanism of symmetry breaking has long remained elusive. Although Nodal proteins of the Transforming Growth Factor β superfamily have long been known to control LR asymmetry in all deuterostome and some protostome species^{2,3}, it is only recently that the unconventional type I Myosin Myosin1D (Myo1D) has emerged as a potentially universal regulator of animal LR asymmetry^{4–7}. Here, we identify the closely related protein Myosin1G (Myo1G) as a positive regulator of the Nodal signaling pathway.

Seminal studies in the mouse revealed the existence of a central LR Organizer (LRO) in which the Planar Cell Polarity (PCP)-dependent orientation of motile cilia promotes the generation of a directional symmetry-breaking fluid flow^{8–10}. Symmetry-breaking cilia-driven fluid flows are also present in other species, including fish and frogs^{11,12}. Already within the vertebrate phylum, the LROs of birds and reptiles do, however, lack motile cilia and rely - at least in chick - on lateralized cell flows to trigger symmetry breaking^{13,14}. Additional mechanisms implicated in LR asymmetry include ion flows¹⁵ and Actin-dependent

chiral cell remodeling^{16,17}. While an increasing number of studies indicate that Actin- and PCP-dependent pathways lie at the core of a symmetry-breaking toolbox^{4,5,18–22}, our understanding of the evolutionary conservation of the mechanisms controlling LR asymmetry remains fragmentary.

In vertebrates, Nodal ligands convey laterality information from the central LRO to target tissues^{1,2}. Nodal ligands propagate on the left side of the embryo by inducing their own expression, allowing them to propagate from the posteriorly located LRO to more anterior target tissues²³. In species with an LRO bearing motile cilia, Nodal is expressed initially in a bilaterally symmetric fashion at the LRO, together with the TGF β signaling antagonist Dand5²⁴. Upon establishment of a ciliary LRO flow, *dand5* transcripts are degraded on the left side of the LRO^{25–27}, allowing Nodal to travel to the left lateral plate mesoderm and propagate by autoinduction.

Nodal ligands induce cellular responses through ligand/receptor complexes that comprise TGF β type I and II receptors and the co-receptor Cripto/Oep²⁸. Nodal ligand binding causes type II receptors to phosphorylate and activate their type I counterpart. A population of endosomes positive for the TGF β signaling adapter Smad Anchor for Receptor Activation (SARA) promotes signal transduction by allowing Activin/Nodal receptors to recruit their transcriptional downstream mediators SMAD2 and 3²⁹. Upon phosphorylation by

¹Université Côte d'Azur, CNRS, Inserm, iBV, Nice, France.  e-mail: maximilian.furthauer@univ-cotedazur.fr

activated type I receptors, SMAD2 & 3 associate with SMAD4 to enter the nucleus and activate target genes²³. As Nodal ligands are highly potent, tight regulation of Nodal signaling is essential not only for embryonic development but also to avoid tumorigenesis^{23,30}. Lefty proteins act as feedback inhibitors of Nodal signaling that prevent the formation of productive ligand/receptor complexes^{23,31}. In LR asymmetry, Lefty expression at the embryonic midline is important to form a barrier that prevents the spreading of left-sided Nodal ligands to the contralateral side^{32,33}.

The requirement of Nodal ligands for LR asymmetry is, however, not universally conserved¹, and a number of protostomian species, including the fruitfly *Drosophila*, altogether lack *nodal* homologs. Studies in *Drosophila* identified MyoID as a master regulator of LR asymmetry^{34,35}. In contrast to the central LRO of vertebrate organisms that governs LR asymmetry of all lateralized organs, *Drosophila myo1d* acts in a local, tissue-autonomous fashion to control genital and visceral laterality^{18,35}. Of particular interest, studies in frogs, fish and humans showed that MyoID is also required for vertebrate LR asymmetry⁴⁻⁷.

Zebrafish MyoID is required for the establishment of a functional symmetry-breaking ciliary LRO flow⁵. In addition to *myo1d*, the fish genome harbors the closely related gene *myosin1g* (*myo1g*). Although *myo1g* mutations impair laterality and enhance the defects of *myo1d* mutants, we show in this work that Myo1G acts independently of the LRO flow, through an entirely different mechanism. We provide evidence that Myo1G represents a positive regulator of the Nodal signaling pathway whose function is essential for the Nodal-mediated transfer of laterality information.

Results

Myosin1G mutants present tissue-specific left-right asymmetry defects

MyoID controls cilia orientation in the LRO to promote the generation of a symmetry-breaking LRO flow⁴⁻⁶. The closely related protein Myo1G (79% amino acid similarity) is also required for zebrafish LR asymmetry but has no detectable effect on the LRO flow⁵, suggesting that different type I Myosins regulate LR asymmetry through distinct mechanisms. To address this issue, we performed a detailed characterization of Maternal Zygotic (MZ) *myo1g* single and MZ *myo1d*:MZ *myo1g* double mutants.

The asymmetric morphogenesis of the zebrafish heart becomes first apparent during the process of cardiac jogging, which transforms the cardiac disc that is initially located at the embryonic midline into a leftward point cardiac tube³⁶⁻³⁸. MZ *myo1g* single mutants present defects in the leftward jogging of cardiac progenitors (Fig. 1a and Supplementary Fig. 1), the penetrance of which is further enhanced in MZ *myo1d*:MZ *myo1g* double mutants (Fig. 1a). To study the effect of *myo1g* on brain laterality, we analyzed the expression of the Nodal ligand *cyclops/nodal related 2* (*cyc/ndr2*), its feedback antagonist *lefty1* (*lft1*) and its transcriptional effector *pitx2* which display predominantly left-sided expression in the dorsal epithalamus of wild-type embryos^{33,39,40}. In contrast to the mild defects observed in MZ *myo1d* mutants (Fig. 1b and Supplementary Fig. 2a, b), MZ *myo1g* single mutants displayed a significantly higher proportion of brain laterality defects (Fig. 1b and Supplementary Fig. 2a, b). In contrast to the effect on brain laterality, MZ *myo1g* mutants display normal expressions of *floating head* in the epiphysis (Supplementary Fig. 2c) and of *otx5* in the pineal complex (Supplementary Fig. 2d), demonstrating thereby that *myo1g* loss of function impairs specifically the laterality but not the specification of dorsal forebrain structures. The penetrance of brain laterality defects in MZ *myo1d*:MZ *myo1g* double mutants is similar to the one observed in MZ *myo1g* single mutants, confirming the predominant role of *myo1g* in brain laterality (Fig. 1b and Supplementary Fig. 2a).

In contrast to the effect of *myo1g* on brain laterality, analysis of liver, pancreas and gut laterality using the endodermal marker *foxa1*

failed to reveal visceral LR asymmetry defects in MZ *myo1g* single mutants (Fig. 1c). The observation that MZ *myo1d*:MZ *myo1g* double mutants present visceral laterality defects that are similar to MZ *myo1d* single mutants (Fig. 1c) confirms that *myo1g* is dispensable for the establishment of visceral laterality.

MyoID is required for LRO morphogenesis and the generation of a ciliary fluid flow⁴⁻⁶. Accordingly, MZ *myo1d* mutants present defects at the level of all lateralized organs (Fig. 1a–c and Supplementary Fig. 2a, b). *myo1g* loss of function yields no discernable LRO flow defects⁵ and affects only a subset of organs (Fig. 1a–c and Supplementary Fig. 2a, b), raising the question of whether *myo1g* may control LR asymmetry through a flow-independent and potentially tissue-specific regulation of organ laterality, similar to the situation described for *Drosophila myo1d*^{18,35}.

Myosin1G controls left-right asymmetry independently of the left-right organizer flow

To directly test if Myosin1 proteins exert LRO flow-independent functions in LR asymmetry, we investigated whether the LR asymmetry defects of animals that lack an LRO flow could be further modified by *myosin1* inactivation. To this aim, we generated double and triple mutants to simultaneously inactivate *myo1d* & *g* and the essential regulator of ciliary motility *dnaaf1/lrrc50*⁴¹. Embryos that completely lack a LRO flow, as is the case for *dnaaf1* mutants, display a distinctive randomization of cardiac, brain, and visceral laterality where LR asymmetry is properly established in roughly one-half of the population (*situs solitus*) but inverted in the other (*situs inversus*, Fig. 1a', d, e, f). Only a small fraction of the embryos that lack an LRO flow display an altogether loss of LR asymmetry (i.e., absence of cardiac jogging and brain laterality markers, visceral *situs ambiguus*, Fig. 1a', d, e).

In contrast, animals that lack both an LRO flow and *myo1* function display a different phenotype, where the heart primordium fails to jog to either the left or the right side of the animal in most embryos (Fig. 1a'). *dnaaf1*:MZ *myo1g* double mutants additionally present a lack of asymmetric *pitx2* expression in the dorsal epithalamus that contrasts with the randomization of lateralized gene expression observed in *dnaaf1* single mutants (Fig. 1b, d). In contrast to the effect observed at the levels of the heart and brain, the visceral phenotypes of *dnaaf1* mutant animals are unaffected by the loss of *myo1g* (Fig. 1e, f), confirming that *myo1g* is dispensable for visceral organ laterality.

These findings provide evidence for a LRO flow-independent function of Myosin1 proteins in LR asymmetry. The observations that (i) *dnaaf1*:MZ *myo1g* double mutants present a more pronounced loss of brain laterality than *dnaaf1*:MZ *myo1d* mutants (Fig. 1d) and that (ii) *dnaaf1*:MZ *myo1d*:MZ *myo1g* triple mutants are generally similar to *dnaaf1*:MZ *myo1g* double mutants (Fig. 1a', d, e) suggest that Myo1G exerts a predominant role in the flow-independent control of LR asymmetry.

Myosin1G is required for Nodal pathway gene expression

Myo1 proteins could act in different ways to ensure a tissue-specific control of embryonic LR asymmetry. First, zebrafish *myo1d* & *g* could act in an organ-intrinsic fashion to promote chiral morphogenesis as in *Drosophila*^{18,35}. Second, Myo1 activity could be required for the Nodal-mediated propagation of laterality information from the central LRO to different target tissues.

Already prior to the first morphological manifestations of asymmetric cell movement, the heart primordium displays asymmetries in gene expression in response to Nodal signaling from the left lateral plate mesoderm (LLPM)^{36,37}. Of particular interest, the cardiac primordia of MZ *myo1g* single and MZ *myo1d*:MZ *myo1g* double mutants present a reduced left-sided expression of the Nodal downstream target and feedback inhibitor *lefty2* (*lft2*) that could reflect impaired Nodal signaling (Fig. 2a). Accordingly, the expression of *southpaw* (*spaw*), the zebrafish Nodal ligand responsible for left-sided Nodal

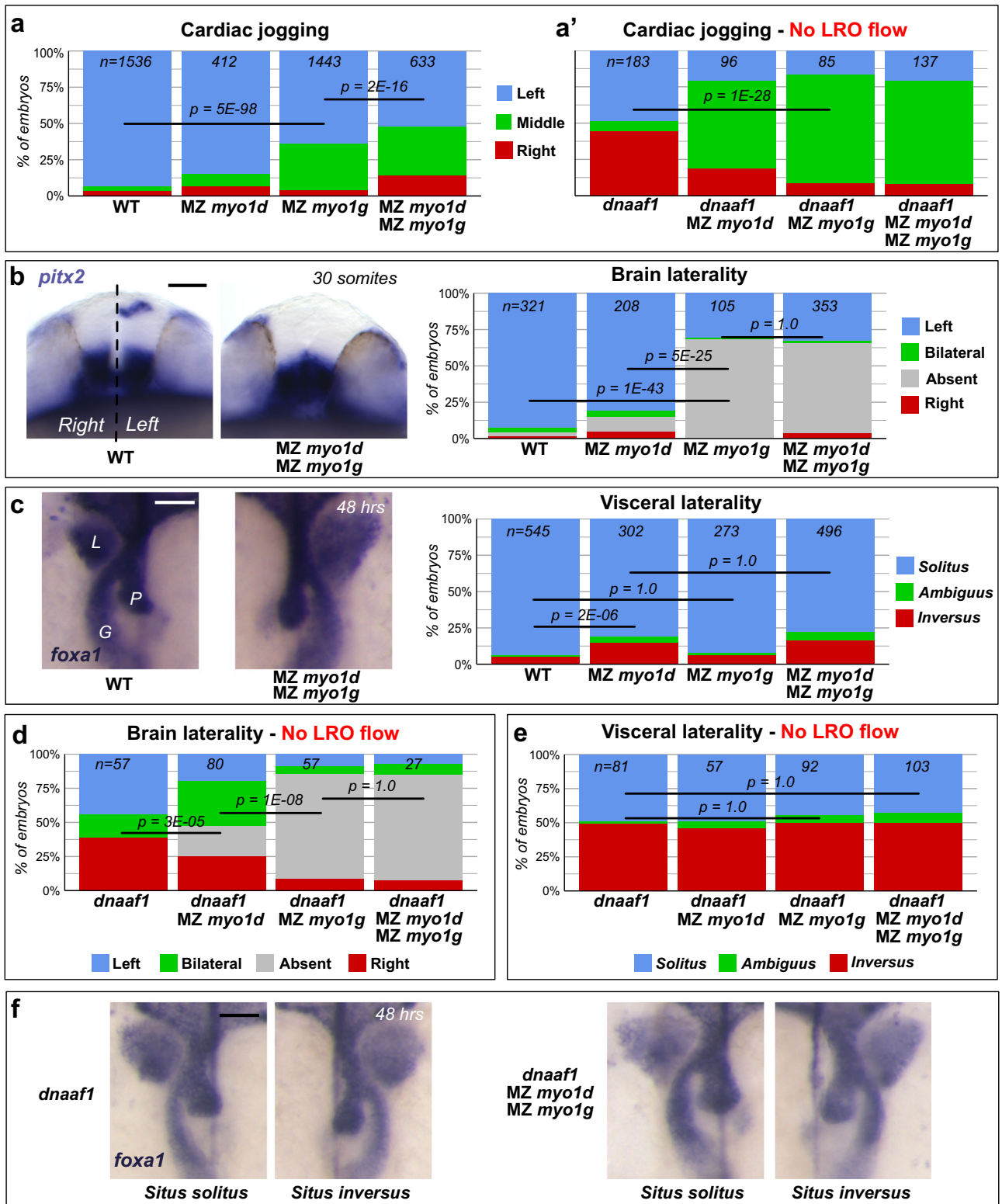


Fig. 1 | Myo1G regulates heart and brain LR asymmetry independent of the LRO flow. **a, a'** Quantification of cardiac jogging indicates that MZ *myo1g* mutants present laterality defects that are enhanced in MZ *myo1d*; MZ *myo1g* double mutants (**a**). Concomitant inactivation of the LRO flow (through *dnaaf1* mutation) reveals that MZ *myo1d/g* mutations enhance the cardiac jogging defects of flow-deficient animals (**a'**). **b** Brain asymmetry is impaired in MZ *myo1g* single and MZ *myo1d*; MZ *myo1g* double mutants. Frontal views of *pitx2* expression at 30 somites, dorsal up. **c** MZ *myo1g* mutants do not show visceral LR defects. L liver, G gut, P

pancreas. Dorsal views of *foxa1* expression at 48 h, anterior up. **d** MZ *myo1d/g* inactivation enhances the brain laterality phenotypes of LRO flow-deficient *dnaaf1* mutants. **e, f** Visceral laterality phenotypes of *dnaaf1* mutants are unaffected by *myo1d/g* inactivation. **f** Dorsal views of *foxa1* expression at 48 h, anterior up. Pictures are derived from the data set quantified in (**e**). Scale bars: 50 μ m. All *p* values were obtained using non-directional statistical tests. Complete numerical and statistical information for all experiments are provided in the Source Data files.

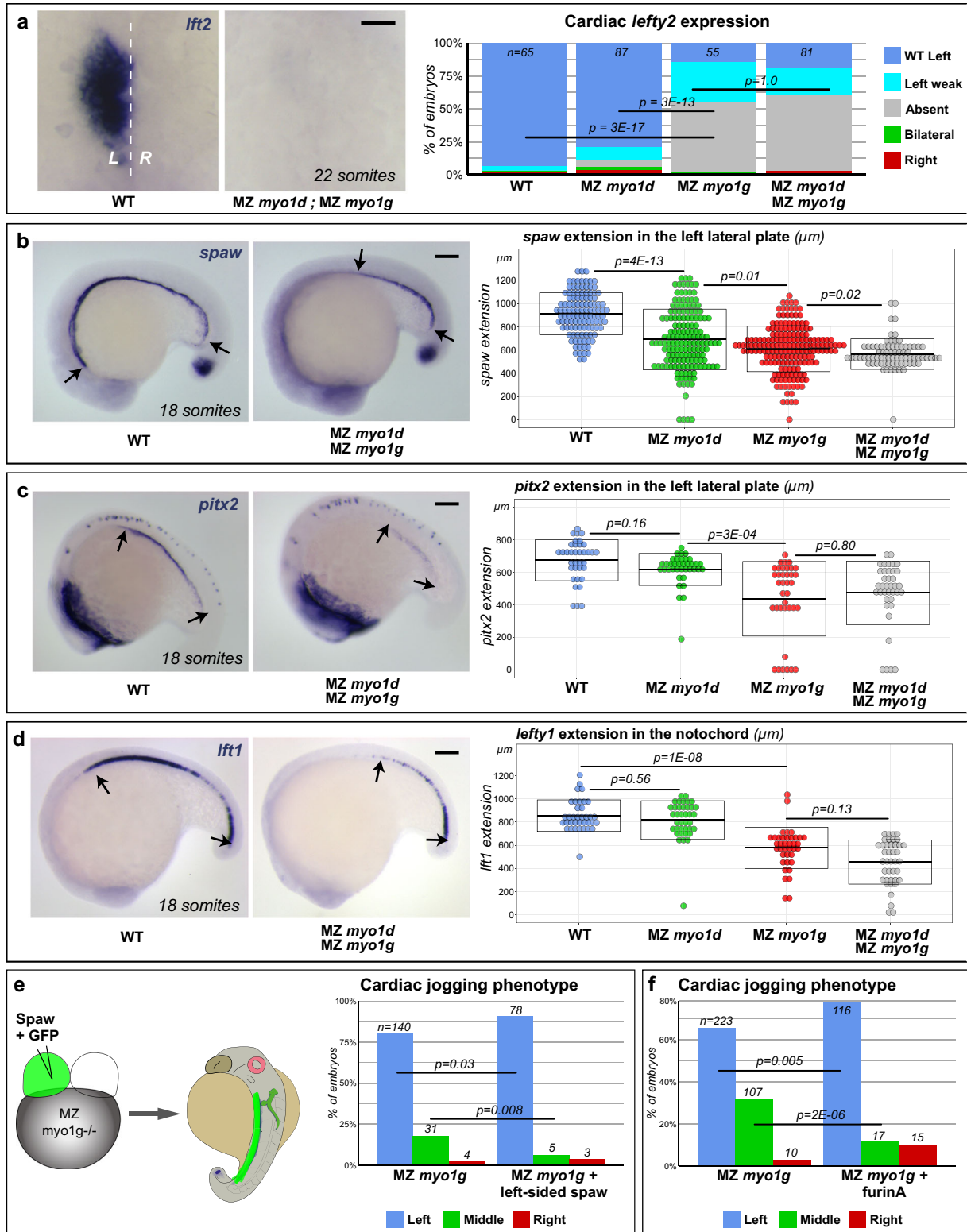


Fig. 2 | MZ *myosin1g* mutants display impaired Nodal signaling. **a** MZ *myo1g* single and MZ *myo1d*; MZ *myo1g* double mutants fail to display asymmetric *lft2* expression in the cardiac primordium. Dorsal views at 22 somites, anterior up. **b–d** MZ *myo1d/g* mutants display a reduced anterior propagation of the expression of the Nodal ligand *spaw* (**b**, see also Supplementary Fig. 3a), the Nodal effector *pitx2* (**c**, see also Supplementary Fig. 3b) and the Nodal feedback inhibitor *lft1* (**d**). Lateral views at 18 somites, anterior left, dorsal up. Box plots in (**b–d**) indicate mean

values \pm SD. **e** Left-sided expression of *Spaw* RNA partially rescues the cardiac jogging defects of MZ *myo1g* mutants (see also Supplementary Fig. 4a, b). **f** Enhancing *Spaw* signaling through furinA RNA injection similarly rescues the cardiac jogging defects of MZ *myo1g* mutants. Scale bars: **a** 50 μm , **b–d** 100 μm . All *p* values were obtained using non-directional statistical tests. Complete numerical and statistical information for all experiments are provided in the Source Data files.

signaling, is reduced and extends less anteriorly in the LLPM of MZ *myo1g* single and MZ *myo1d*; MZ *myo1g* double mutants, while being affected to a lesser degree in MZ *myo1d* single mutants (Fig. 2b and Supplementary Fig. 3a). In further accordance with impaired Nodal signaling, *myo1*-deficient animals display a reduced expression of the Nodal-targets *pitx2* and *elovl6* in the LLPM (Fig. 2c and Supplementary Fig. 3b, c) and a reduced extension of the Nodal feedback inhibitor *lftl* in the notochord that provides a molecular midline barrier for lateralized Nodal signaling (Fig. 2d).

Promoting Nodal signaling restores cardiac laterality in MZ *myosin1g* mutants

If the LR asymmetry defects of MZ *myo1g* mutant animals are due to impaired Nodal signaling, augmenting left-sided Nodal signaling should allow for rescue cardiac laterality. To test this hypothesis, Spaw and GFP RNAs were co-injected into a single blastomere at the two-cell stage. By the end of gastrulation, the GFP tracer allowed to select animals in which the progeny of the injected blastomere was restricted to either the left or the right side of the embryo. In accordance with a potential requirement for *myo1g* in Nodal signaling, left-sided Spaw expression allowed to significantly decrease the number of MZ *myo1g* mutants for which the primordium fails to jog and stays at the midline and increase the percentage of MZ *myo1g* mutants that present a proper leftward cardiac jogging (Fig. 2e). In contrast, the chirality of cardiac looping, a process that subsequently generates the atrial and ventricular chambers and occurs largely independently of Nodal signaling⁴² was not restored by left-sided Spaw expression (Supplementary Fig. 4b). Animals in which Spaw-injected cells ended up on the right side of the embryo display aggravated cardiac jogging and looping defects compared to non-injected MZ *myo1g* mutants (Supplementary Fig. 4a, b).

Spaw activity is controlled by the proprotein convertase FurinA which promotes the cleavage of the Spaw prodomain to allow the formation of a mature ligand⁴³. We, therefore, used furinA over-expression, which has previously been shown to extend the Spaw signaling range⁴³, as an alternative strategy to increase Spaw signaling in MZ *myo1g* mutants. furinA-injected MZ *myo1g* mutants present a significantly reduced number of cardiac jogging defects compared to non-injected siblings (Fig. 2f), indicating again that MZ *myo1g* mutants can be partially rescued by promoting Nodal signaling. Finally, genetic analysis reveals that the cardiac jogging phenotypes of animals that are already devoid of Maternal and Zygotic *spaw* function (MZ *spaw* mutants) are not further modified by the loss of *myo1g* in MZ *spaw*; MZ *myo1g* double mutants (Supplementary Fig. 4c), in accordance with the hypothesis that Myo1G exerts a Spaw-dependent control of LR asymmetry.

The left-right organizer flow and *myosin1* genes control Nodal propagation

Through its ability to promote the unilateral degradation of transcripts encoding the Nodal signaling antagonist Dand5, the LRO flow enables the left-sided propagation of *nodal* expression^{25–27}. Our observation that Myo1G and (to a lesser degree) Myo1D act to promote the propagation of *spaw* expression (Fig. 2b and Supplementary Fig. 3a) raises the question of whether the enhanced laterality defects of embryos that lack both an LRO flow and *myo1* gene function (Fig. 1) could be due to cumulative effects on *nodal* gene expression? To address this issue, we performed a comparative quantitative analysis of *spaw* expression in the Lateral Plate Mesoderm (LPM) of embryos that lack an LRO flow (due to *dnaaf1* inactivation) as well as *myo1d* & *g* activities.

In wild-type control embryos, *spaw* extends anteriorly up to the level of the heart and brain primordia in the left LPM, while its expression is either entirely absent or only restricted to the posterior-most LPM on the right side of the embryo (Fig. 3a). Morpholino-mediated knock-down of *dnaaf1* (Fig. 3a) or its genetic inactivation

(Fig. 3b) cause a reduction in the left-sided extension of *spaw* which is likely due to a failure to downregulate *dand5* on the left side of the LRO. Additionally, *dnaaf1*-deficient animals present a roughly symmetric expression of *spaw* in the right LPM (Fig. 3a, b). Simultaneous inactivations of *myo1d/g* and *dnaaf1* cause a further reduction of the anterior extension of *spaw* expression on both the left and the right side of the animal (Fig. 3a, b), demonstrating thereby that Myosin1 proteins exert a flow-independent control of *nodal* ligand expression. Similar results were obtained using *dnaaf1* morphants or mutants, although quantitatively stronger effects are observed upon the use of stable genetic mutants compared to transient morpholino knock-down. In accordance with our morphological analysis of embryonic laterality that suggested a predominant role of Myo1G in the LRO flow-independent control of LR asymmetry (Fig. 1), the inactivation of *myo1g* has a stronger effect on *spaw* expression in the LPM of *dnaaf1*-depleted animals than the loss of function of *myo1d* (Fig. 3a, b).

Nodal expression fails to reach the cardiac primordium in MZ *myosin1g* mutants

Spaw-mediated Nodal signaling is required to transmit laterality information from the LRO to target tissues. The zebrafish LRO, Kupffer's Vesicle⁴⁴ is located at the posterior tip of the notochord. Among the different tissues undergoing chiral morphogenesis, the visceral organ primordia are closest to the LRO, while heart and brain primordia are located more anteriorly at increasing distances. As our experiments show that MZ *myo1g* mutants present no defects in visceral LR asymmetry but increasingly severe phenotypes in the more anterior heart and brain (Fig. 1a–c), we wondered whether the reduced extension of left-sided *spaw* expression (Fig. 2b) may result in a failure to reach more anteriorly located organ primordia. To test this hypothesis, we performed two color in situ hybridization to simultaneously visualize *spaw* expression and the *cmhc2/myl7*-positive cardiac primordium.

Our analysis reveals that by the 22 somites stage, *spaw* expression has reached the cardiac primordium in most wild-type embryos (Fig. 3c, c' and Supplementary Fig. 5a, a'). Similarly, *spaw* extends up to the level of the heart primordium on either the left, the right, or both sides of the embryo in most animals that are mutant or morphant for the LRO flow regulator *dnaaf1* (Fig. 3c, c' and Supplementary Fig. 5a, a'). In contrast, *spaw* expression fails to reach the cardiac primordium in a significant fraction of MZ *myo1g* mutants (Fig. 3c, c' and Supplementary Fig. 5a, a'), providing thereby a potential explanation for their cardiac jogging defects. Compound inactivations of *dnaaf1* and *myo1g* result in near complete failure of *spaw* expression to reach the cardiac primordium (Fig. 3c, c' and Supplementary Fig. 5a, a'), in accordance with the predominant lack of cardiac jogging that is observed in these animals (Fig. 1a').

Our experiments show that in MZ *myo1g* mutants, *spaw* expression frequently fails to extend anteriorly to reach the cardiac (Fig. 3c and Supplementary Fig. 5) and, therefore, necessarily also the even more anterior brain primordium, providing an explanation for the laterality defects that are observed in these two tissues (Fig. 1a, b). Conversely, the residual *spaw* expression of MZ *myo1g* mutants still extends up to the level of the posterior gastrointestinal tract (Supplementary Fig. 6), a fact that may explain the observation the visceral laterality is correctly established in these animals (Fig. 1c).

MZ *myosin1g* mutants display a temporal delay in *spaw* expression

To investigate the mechanism through which *myosin1* genes contribute to the LRO flow-independent regulation of Nodal signaling, we performed a time-course analysis of *spaw* expression during development. As *myo1d* contributes to both the regulation of the LRO flow⁵ and the flow-independent control of *nodal* expression (Fig. 3), we focused our analysis on *myo1g*, which plays a predominant role in the flow-independent control of Nodal signaling (Figs. 1, 3).

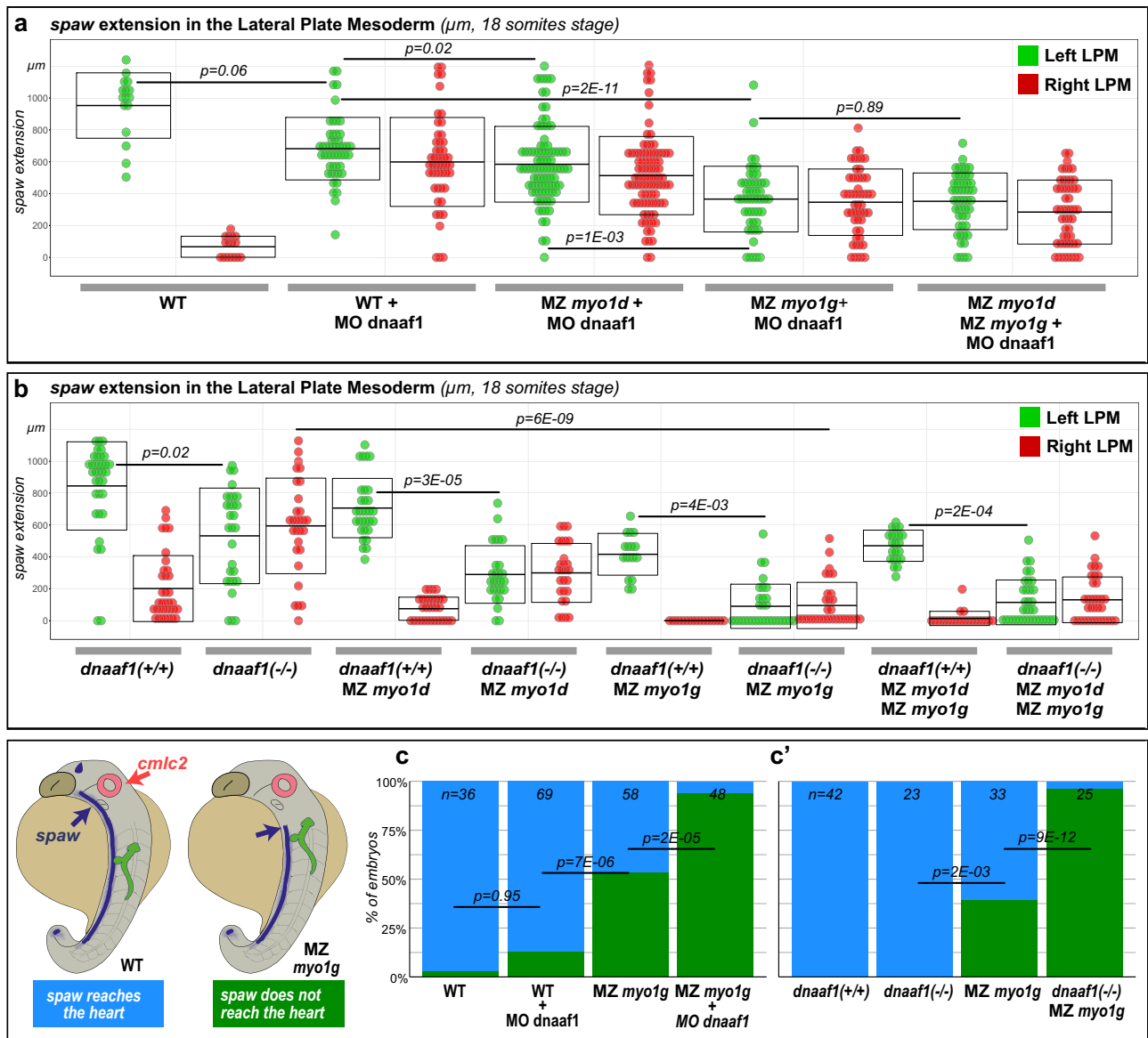


Fig. 3 | MyosinI proteins regulate *spaw* expression independently of the LRO flow. a Quantification of *spaw* extension in the Left (green dots) and Right (red dots) LPM of 18 somites stage LRO flow-deficient *dnaaf1* morphant (a) or *dnaaf1* mutant (b) embryos. *myo1d/g* loss of function causes a significant reduction of the antero-posterior extension of *spaw* expression in both the Left and the Right LPM. To allow direct comparison, mutant animals in a, b are derived from the same genetic background. Box plots in a, b indicate mean values \pm SD. c, c' Double in situ

hybridization for *spaw* and the cardiac marker *cmlc2/myl7* (see Supplementary Fig. 5 for pictures) reveals that *spaw* expression reaches the cardiac primordium in most WT control and LRO flow-deficient *dnaaf1* morphant (c) or *dnaaf1* mutant (c') embryos, but fails to do so upon inactivation of *myo1g*. All p values were obtained using non-directional statistical tests. Complete numerical and statistical information for all experiments are provided in the Source Data files.

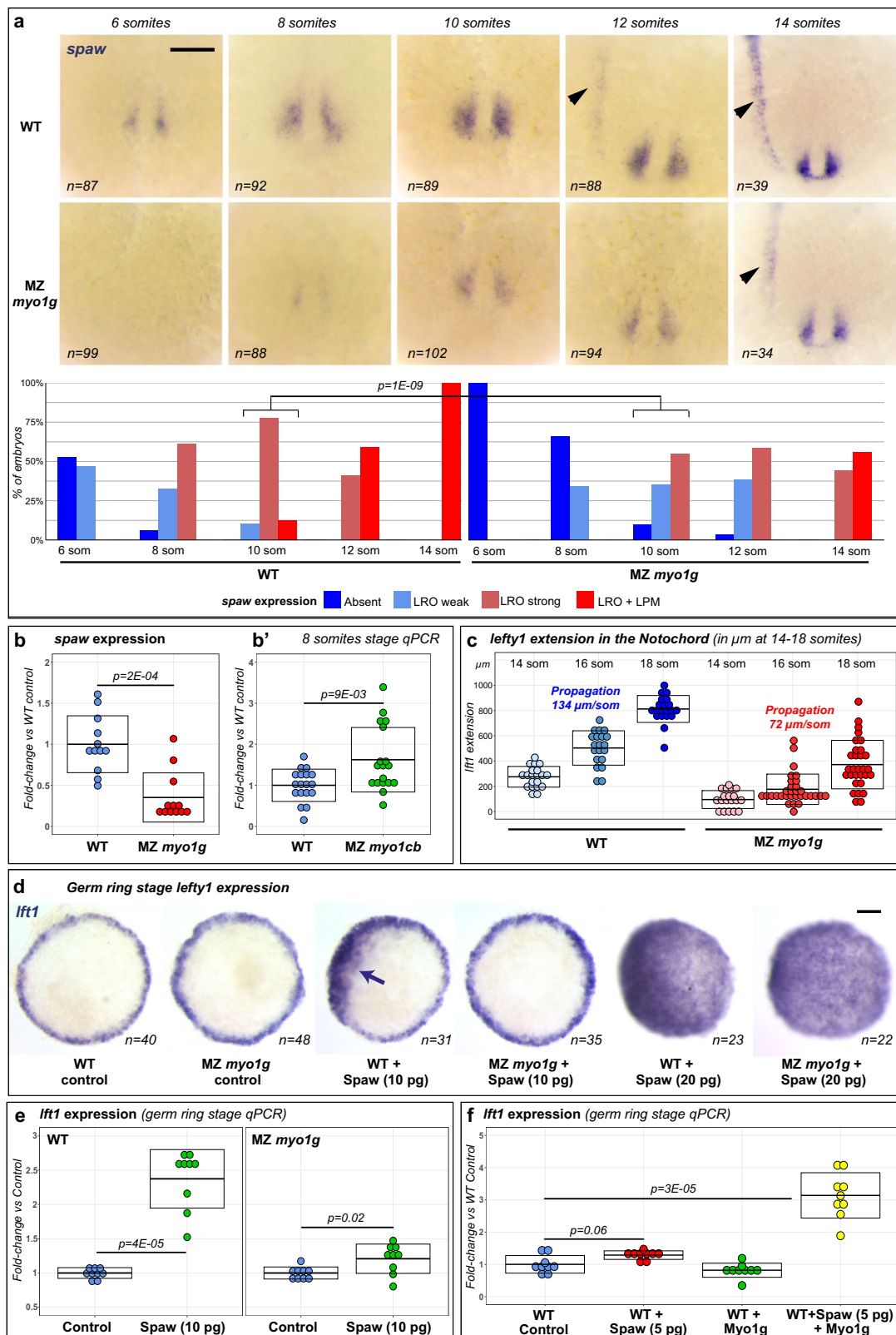
In wild-type embryos, *spaw* expression is initiated bilaterally in the cells that surround the LRO by the six somites stage (Fig. 4a). As development proceeds, *spaw* LRO levels increase until at around the 12 somites stage expression also becomes detectable in the left LPM where the ligand then propagates through autoinduction to reach more anterior target tissues (Fig. 4a). Analysis of *spaw* expression in MZ *myo1g* mutants revealed a temporal delay in the emergence of *spaw* expression at the level of the LRO and the subsequent propagation to the LPM (Fig. 4a). In contrast to the loss of *myo1g* function, a lack of LRO flow upon depletion of *dnaaf1* is without effect on the initial induction of *spaw* expression at the LRO (Supplementary Fig. 7a).

The observation that MZ *myo1g* mutants present a reduced *spaw* expression at the LRO was confirmed by quantitative qRT-PCR (Fig. 4b). Studies in *Drosophila* and zebrafish revealed that

Myosin1C (Myo1C) proteins can act as Myo1D/G antagonists^{5,44}. Although our analysis failed to reveal any morphological LR asymmetry defects in Maternal Zygotic *myo1Cb* mutants, gene expression analysis uncovered a mild upregulation of *spaw* at the LRO (Fig. 4b' and Supplementary Fig. 7b), supporting the functional relationship between Myo1D/G agonists and their Myo1Cb antagonist.

***myosin1g* is dispensable for left-right organizer formation**

The finding that zebrafish *myo1d* is required for LRO morphogenesis^{5,6} raises the question of whether the loss of *myo1g* may similarly cause general defects in LRO morphogenesis that would ultimately result in reduced Nodal signaling at the LRO. Our analysis of different markers genes involved in LRO specification and function does, however, not support this hypothesis. Analysis of the endodermal markers *sox17* and



sox32 indicates that the specification and clustering of LRO precursor cells occur normally in MZ *myo1g* mutants (Supplementary Fig. 8a, b). In accordance with the fact that *myo1g* controls LR asymmetry independently of the LRO flow, *myo1g* loss of function has no effect on the expression of the ciliary motility genes *foxj1a*, *dnah9*, and *odad1* (Supplementary Fig. 8c–e).

Myosin1G promotes Nodal signaling

In mice and zebrafish, Nodal expression at the LRO is initially induced by Notch signaling⁴⁵, and then further upregulated through the capacity of Nodal ligands to induce their own expression⁴⁶. While the analysis of the Notch target genes *her4.1* and *her15.1* suggests that MZ *myo1g* mutants present normal Notch signaling levels (Supplementary

Fig. 4 | Myo1G promotes Spaw signaling. **a** Time-course analysis of *spaw* expression indicates that initiation of *spaw* expression at the LRO and propagation to the Left LPM (black arrowhead) are delayed in MZ *myo1g* mutants. Vegetal views of the LRO region, anterior up. **b, b'** qPCR analysis of *spaw* expression confirms that *spaw* levels are significantly reduced in MZ *myo1g* mutants (**b**). Conversely, *spaw* expression increases in Maternal Zygotic *myo1cb* (MZ *myo1cb*) mutants (**b'**, see also Supplementary Fig. 7b). **c** MZ *myo1g* mutants present a significantly reduced ($p = 2E-05$) rate of anterior-ward propagation of *lft1* expression in the notochord (see also Supplementary Fig. 9a). **d, e** MZ *myo1g* mutants display a weaker induction of the nodal target gene *lft1* in response to Spaw overexpression. **d** Animal pole views of germ ring stage embryos. While high amounts (20 pg) of Spaw RNA induce

a similar *lft1* induction in MZ *myo1g* mutants and wild-type controls, *myo1g*-deficient embryos present a reduced response to moderate amounts (10 pg) of Spaw RNA (arrow indicates ectopic expression, see Supplementary Fig. 9b for quantification). **e** qPCR analysis confirms that equal amounts of Spaw RNA induce a reduced *lft1* induction response in MZ *myo1g* mutants compared to WT Control embryos from the same genetic background. **f** Conversely, the overexpression of Myo1G potentiates the capacity of low amounts (5 pg) of Spaw RNA to induce ectopic *lft1*. Scale bars: 100 μ m. Box plots in **b, b', c, e, f** indicate mean values \pm SD. All p values were obtained using non-directional statistical tests. Complete numerical and statistical information for all experiments are provided in the Source Data files.

Fig. 8f, g), the reduced expression of *spaw* at the LRO (Fig. 4a) is similar to the one reported in animals mutant for *spaw* itself¹⁶.

Following the initiation of *spaw* expression, first at the level of the LRO and subsequently in the LPM, *spaw* propagates anteriorly through autoinduction. This posterior-to-anterior propagation is accompanied by the progressive induction of the nodal feedback-antagonist *lft1* at the notochordal midline barrier^{32,33,46}. Our data show that in addition to the delayed expression of *spaw* at the LRO and in the LLPM (Fig. 4a), MZ *myo1g* mutants present a nearly two-fold reduction in the rate of anterior propagation of notochordal *lft1* expression (Fig. 4c and Supplementary Fig. 9a).

As Nodal ligands amplify their own expression by autoinduction as soon as they start to be expressed²³, it is not possible to determine if the delays that we observe in *spaw* and *lft1* expression are due to a defect in the initial induction of *spaw*, to a subsequent defect in *spaw* autoinduction or to a combination of the two. To circumvent this problem, we took advantage of germ ring stage embryos, which lack endogenous *spaw*, to introduce defined amounts of *spaw* RNA by microinjection and compare nodal target gene induction in WT control and MZ *myo1g* mutant animals. While high doses (20 pg) of Spaw readily induce ectopic *lft1* expression in both WT and MZ *myo1g* mutants (Fig. 4d and Supplementary Fig. 9b), mutant animals present a reduced response to moderate (10 pg) doses of Spaw RNA (Fig. 4d and Supplementary Fig. 9b). Analysis of *lft1* expression by quantitative RT-PCR reveals that while Spaw is still able to significantly induce *lft1* in MZ *myo1g* mutants, the observed effect is weaker than in homozygous WT sibling controls (Fig. 4e, Cohen's d effect size = 1.27 for MZ *myo1g* mutants versus 4.48 for WT controls).

Taken together, our observations suggest that Myo1G, while not strictly required for Spaw signal transduction, is essential to promote full-strength Nodal signaling. Injecting wild-type Myo1G RNA into MZ *myo1g* mutants significantly rescues the capacity of Spaw to induce *lft1* expression, demonstrating the specificity of the observed effect (Supplementary Fig. 9c). To confirm that Myo1G promotes Spaw signaling, a lower amount of Spaw RNA (5 pg), that is on its own barely capable of inducing ectopic *lft1* expression, was co-injected with wild-type Myo1G RNA into WT animals. qRT-PCR analysis shows that Myo1G overexpression promotes the capacity of this subliminal amount of Spaw to induce *lft1* expression (Fig. 4f).

Myosin1G function in Southpaw-independent Nodal signaling

The observation that germ ring stage *myo1g*-deficient animals display a reduced induction of the nodal target gene *lft1* in response to ectopic Spaw (Fig. 4d, e) raises the question whether Myo1G might also contribute to signaling mediated by *cyclops* (*cyc*) and *squint* (*sqt*), the two zebrafish nodal ligands that are responsible for the endogenous expression of *lft1* in blastula/gastrula stage embryos.

The same experimental setup that has allowed us to show that Myo1G enhances Spaw activity (Fig. 4d and Supplementary Fig. 9b) was used to test if Myo1G also enhances Cyc / Sqt signaling. Our experiments show that while the injection of high doses of *cyc* or *sqt* RNA is sufficient to induce ectopic *lft1* expression in WT as well as MZ *myo1g* mutant animals, mutant animals present a reduced response to

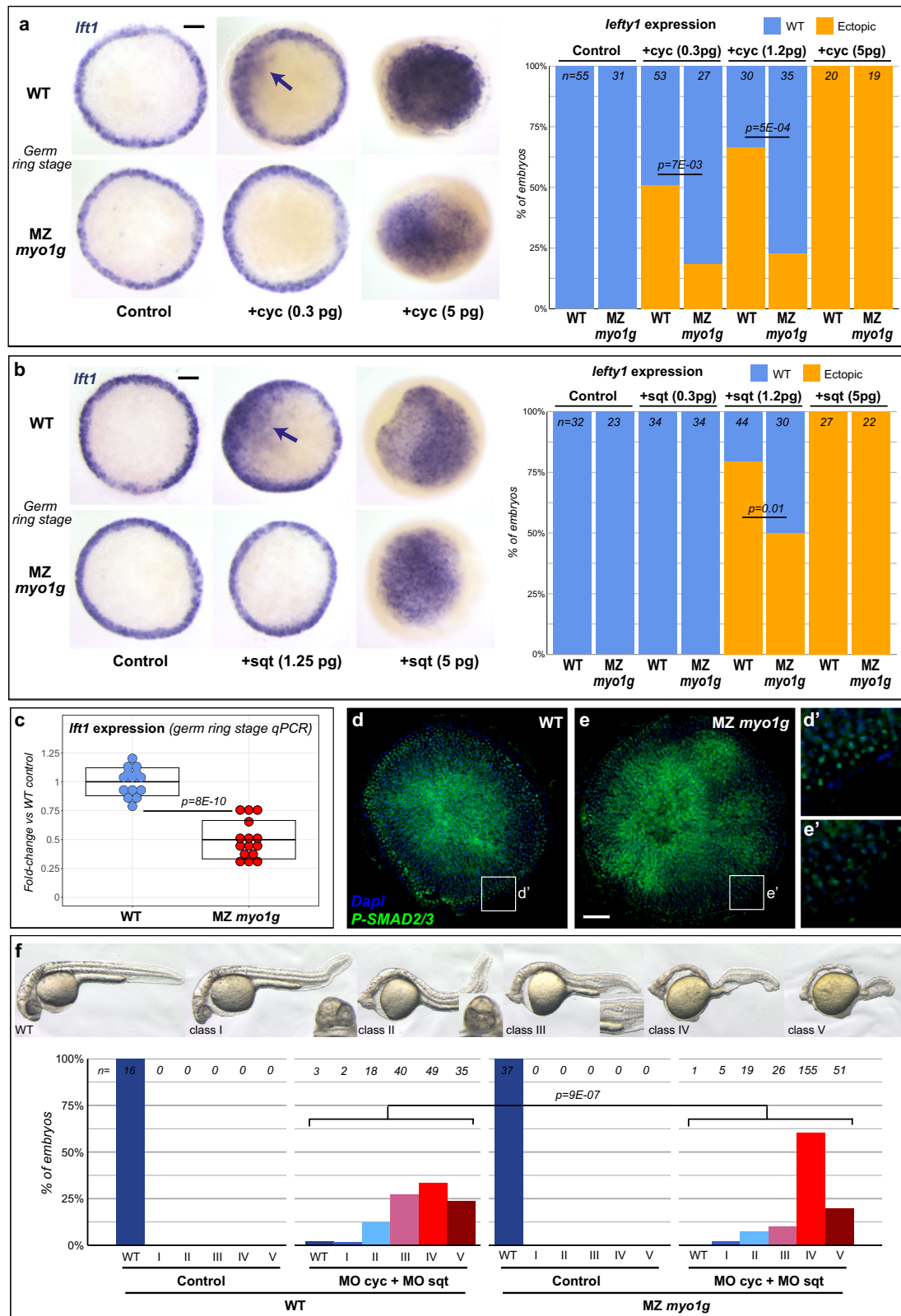
moderate doses of *cyc/sqt* RNA (Fig. 5a, b). These observations indicate that, as already observed for Spaw, Myo1G is not strictly required for signaling by Cyc and Sqt but enhances the response to the ectopic expression of these Nodal ligands.

In the context of LR asymmetry, MZ *myo1g* mutants present a number of molecular and morphological phenotypes that are compatible with a reduction in Spaw-mediated Nodal signaling (Figs. 1, 2). In contrast, examination of MZ *myo1g* mutants using molecular markers (e.g., gastrulation stage endodermal *sox17* expression, Supplementary Fig. 8a) or morphological examination failed to reveal any of the diagnostic phenotypes that are caused by defects in *cyc/sqt*-mediated germ layer specification (cyclopia or loss of axial structures, Fig. 5f)^{40,47,48}. In spite of this lack of morphological phenotypes, germ ring stage MZ *myo1g* mutants present a partial reduction of *lft1* expression that is detectable by qPCR (Fig. 5c) and a diminished immunoreactivity for activated Phospho-SMAD2/3 (Fig. 5d, e). These observations suggest that Myo1G does contribute to endogenous blastula stage *cyc/sqt* signaling, but that its importance for this process is only minor and *myo1g* loss of function therefore not associated with visible defects in Nodal-dependent germ layer specification. In accordance with a minor contribution of Myo1G to early *cyc/sqt* signaling, we observe a weak enhancement of the Nodal loss of function phenotypes that are observed upon partial *cyc/sqt* morpholino knock-down in MZ *myo1g* mutants compared to WT controls (Fig. 5f).

Taken together, our experiments indicate that in spite of its ability to promote *cyc/sqt* signaling (Fig. 5a, b) Myo1G is only of minor importance for Nodal signaling during the early blastula/gastrula period. In contrast, our analysis shows that by the end of gastrulation (bud stage), MZ *myo1g* mutants present a clear reduction of *lft1* which is at this stage expressed together with *cyc* at the level of future LRO (Fig. 6a). This phenotype is observed more than 2 h before the onset of the expression of *spaw* itself, suggesting thereby that MZ *myo1g* mutants present a defect in *cyc* signaling/autoinduction that becomes detectable by the end of gastrulation.

In addition to the effect observed on *lft1* and *cyc*, MZ *myo1g* mutants present a reduced expression of the Cerberus/Dan family member *dand5* that antagonizes *spaw* signaling at the LRO²⁴ (Fig. 6b) as well as the TGF β superfamily member *gdf3* that represents an obligate heterodimerization partner of different Nodal ligands, including Spaw⁴⁹ (Fig. 6a). It is important to note that markers of LRO specification (*sox17*, *sox32*, *foxj1a*), LRO differentiation (*dnah9*, *odad1*), or other LRO signaling pathways (*her4.1*, *her15.1*) remain expressed normally (Supplementary Fig. 8), arguing that the observed defects in nodal pathway gene expression reflect a specific impairment in Nodal signaling and autoinduction rather than a general problem of LRO morphogenesis. In accordance with this hypothesis, morpholino knock-down of *cyc* or *sqt* or the genetic inactivation of *spaw* itself similarly cause a partial loss of *gdf3* expression at the LRO (Supplementary Fig. 10).

Importantly our experiments indicate that Myo1G regulates Nodal signaling not only in the context of LR asymmetry, as eight-somites stage MZ *myo1g* mutants also present a reduced expression of *lft1* in the anterior brain, which lacks *spaw* but expresses *cyc*^{39,40} (Fig. 6c). Taken together, our findings suggest that while Myo1G is essential for



the Spaw-mediated establishment of zebrafish LR asymmetry, it also contributes to signaling by other Nodal ligands in specific biological contexts.

Myosin1G regulates activin receptor trafficking

How does Myo1G promote Spaw signaling? Proteomic studies identified Myo1G on exosomes, suggesting that this factor may be implicated

in exovesicular secretion⁵⁰. To determine if Myo1G is required for Spaw ligand secretion, we took advantage of a functional GFP-Spaw fusion protein construct that has been previously used to visualize Spaw secretion⁴³. GFP-Spaw RNA injection into wild-type or MZ *myo1g* mutant animals results in similar labeling of the extracellular space (Fig. 7a, b). For quantitative assessment of Spaw-GFP levels, Spaw-GFP RNA was co-injected with a Histone2B-RFP RNA that enabled us to estimate the

Fig. 5 | Myo1G promotes signaling by different Nodal ligands. **a, b** MZ *myo1g* mutants display reduced *lft1* induction in response to ectopic expression of the Nodal ligands cyclops (*cyc*, **a**) and squint (*sqt*, **b**). Animal pole views of germ ring stage embryos, arrows indicate patches of ectopic *lft1* expression. **c** qPCR indicates that MZ *myo1g* mutants present a mild decrease in the endogenous expression levels of the Nodal target gene *lft1*. Box plots in **c** indicate mean values \pm SD. **d, e** MZ *myo1g* mutants present a reduced immunoreactivity for activated Phospho-SMAD2/3 ($n = 25$ WT and 31 MZ *myo1g* mutant embryos from 2 independent

experiments). Animal pole views of germ ring stage embryos. Scale bar: 100 μ m. **f** Morpholino knockdown of *cyc* and *sqt* (MO *cyc* + MO *sqt*) elicits stronger Nodal loss of function phenotypes in MZ *myo1g* mutants than in WT controls. Nodal loss of function phenotypes at 32 hpf were categorized into five classes: class I (partial cyclopia), class II (complete cyclopia), class III (partial loss of the notochord), class IV (complete loss of the notochord), and class V (loss of posterior neural structures). All *p* values were obtained using non-directional statistical tests. Complete numerical and statistical information are provided in the Source Data files.

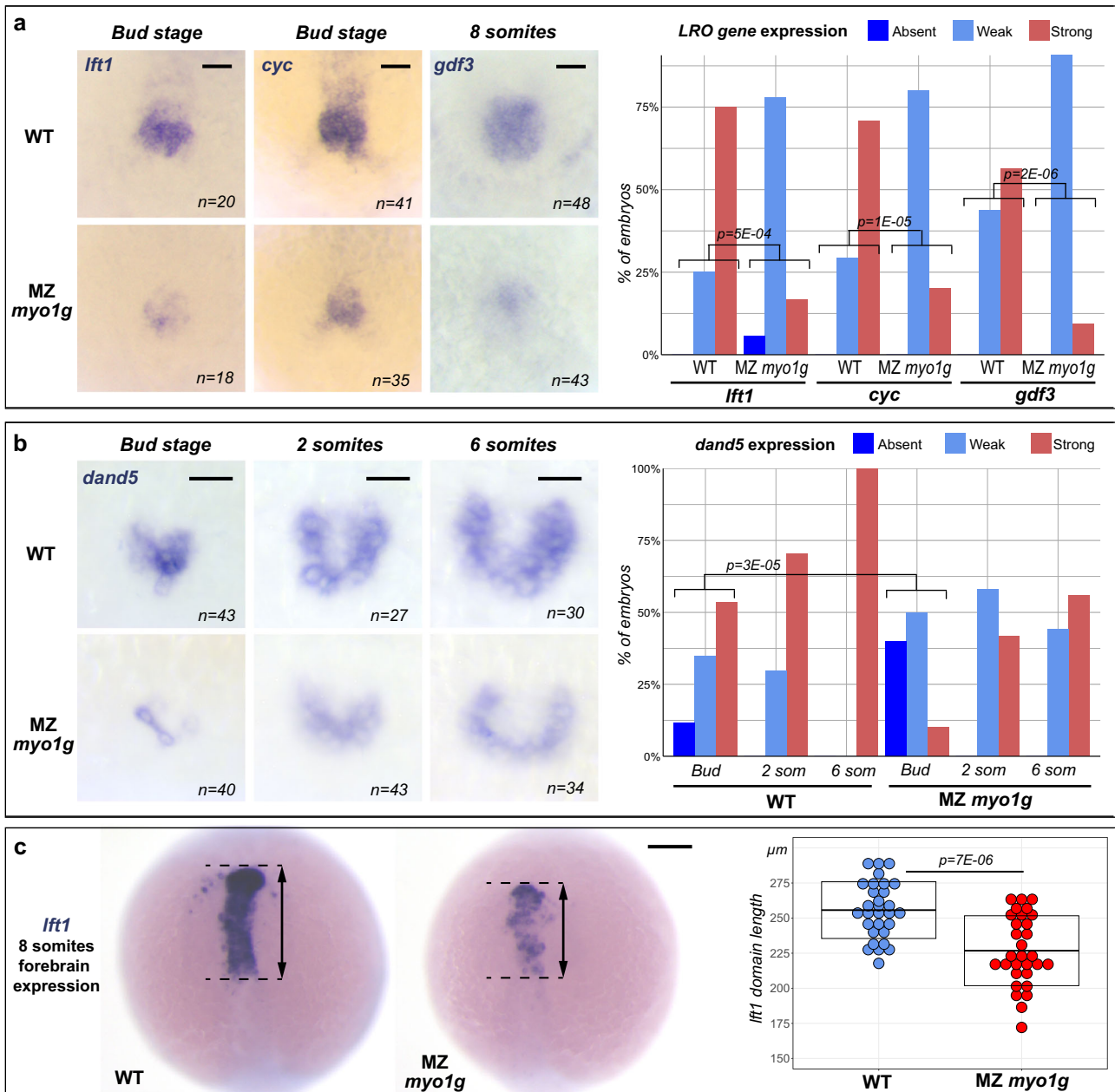


Fig. 6 | Defective Nodal pathway gene expressions in early segmentation stage MZ *myo1g* mutants. **a** MZ *myo1g* mutants present a reduced expression of the Nodal ligand *cyc* and the Nodal feedback antagonist *lft1* in the LRO/tail bud region of bud stage embryos. Mutant embryos also present a reduced expression of the Nodal ligand *gdf3* in the eight-somites stage LRO. **b** MZ *myo1g* mutants display a reduced expression of the Nodal signaling antagonist *dand5* from the bud stage

onwards. **a, b** show vegetal views of the LRO/tail bud region, anterior up. **c** Eight-somites stage MZ *myo1g* mutants present a reduction in the antero-posterior extension of *lft1* expression in the anterior brain. Dorsal views of the brain, anterior up. Box plots in **c** indicate mean values \pm SD. Scale bars: **a** 50 μ m, **b, c** 100 μ m. All *p* values were obtained using non-directional statistical tests. Complete numerical and statistical information are provided in the Source Data files.

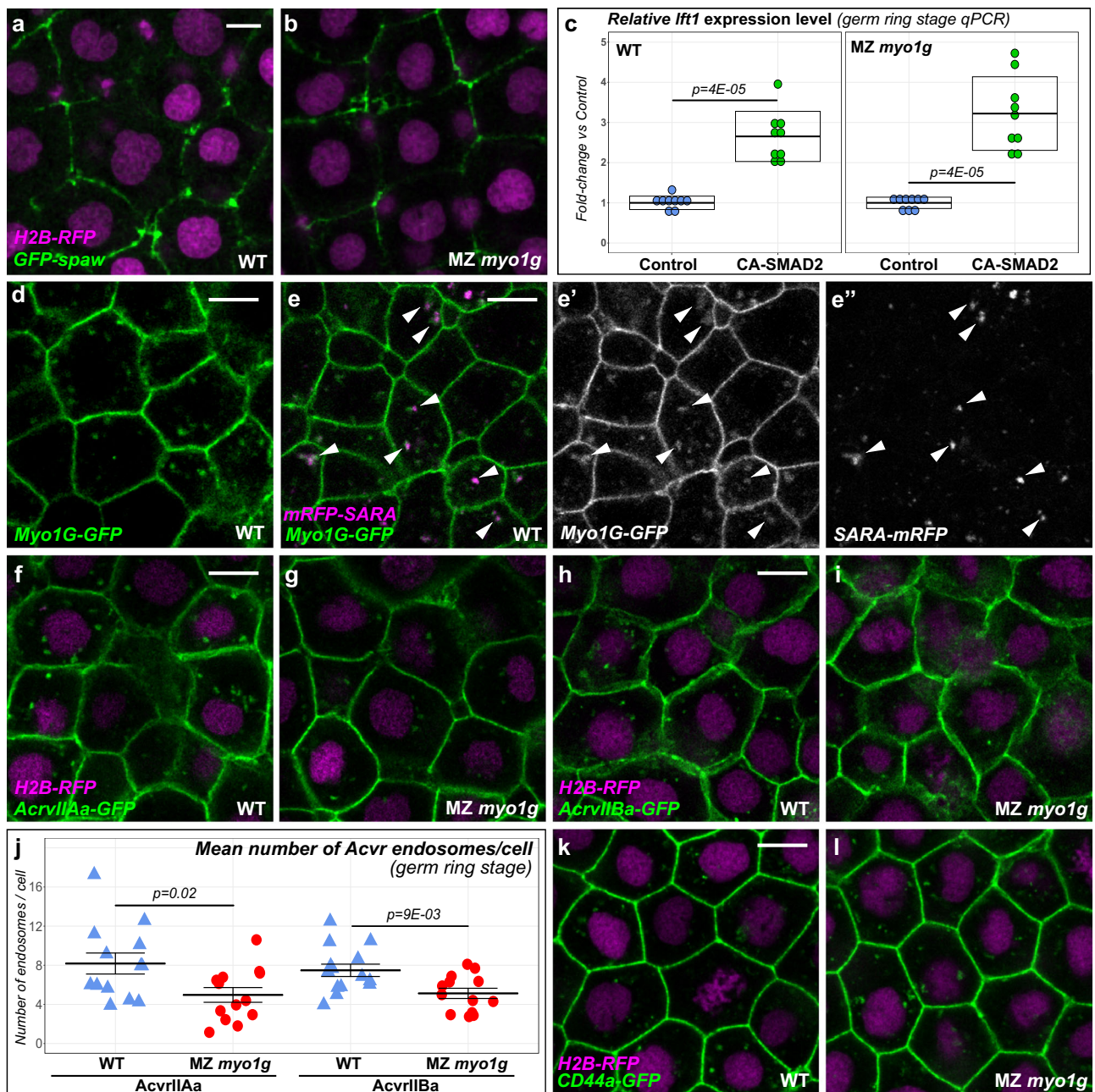


Fig. 7 | Myo1G regulates nodal receptor trafficking. **a, b** Spaw-GFP localization is similar in WT ($n = 20$) and MZ *myo1g* mutants ($n = 17$). H2B-RFP was injected as a tracer to ascertain that embryos that had received equal amounts of RNA (see Supplementary Fig. 11a for quantification). **c** A constitutively activated form of the Nodal signal transducer SMAD2 (CA-SMAD2) elicits similar responses in WT and MZ *myo1g* mutants. Box plots in **c** indicate mean values \pm SD. **d** Myo1G-GFP is detected at the cell cortex and in intracellular compartments ($n = 10$). **e, e', e''** Myo1G-GFP is present on endosomes positive for the TGF β signaling adapter SARA ($n = 24$, see also Supplementary Fig. 12a, b). **f–j** MZ *myo1g* mutants present a reduced number of endosomes positive for the Nodal receptors Acvr2Aa-GFP (**f, g, j**, $n = 13$ WT and 13

MZ *myo1g* mutant embryos) and Acvr2Ba-GFP (**h–j**, $n = 14$ WT and 13 MZ *myo1g* mutant embryos). In **j** data points represent the mean number of endosomes per cell for a particular embryo and lines indicate the overall mean \pm SEM. **k, l** MZ *myo1g* mutants and WT siblings present a similar number of CD44a-positive endosomes ($n = 7$ WT and $n = 7$ MZ *myo1g* mutant embryos, see Supplementary Fig. 11b for quantification). **a, b, d–i, k, l**, animal pole views, germ ring stage. Scale bars: 10 μ m. All p values were obtained using non-directional statistical tests. Complete numerical and statistical information are provided in the Source Data files.

amount of injected material received by individual embryos. Quantification of Spaw levels relative to the Histone2B tracer revealed that while MZ *myo1g* mutants present a minor reduction of normalized Spaw-GFP expression levels, this reduction is not statistically significant, suggesting that Myo1G has no major effect on Spaw ligand production and secretion (Supplementary Fig. 11a).

While cytoplasmic Myosin1 proteins exert important roles in membrane trafficking⁵¹, nuclear isoforms of mammalian Myo1C can

regulate TGF β -responsive gene expression⁵². To determine if Myo1G controls the SMAD-mediated transcriptional downstream response to Spaw signaling, we injected RNA encoding a Constitutively Activated variant of SMAD2 (CA-SMAD2) into wild-type and MZ *myo1g* mutant animals and analyzed the effect on *lft1* target gene induction by qRT-PCR. In contrast to the reduced induction of *lft1* that is observed upon Spaw overexpression in MZ *myo1g* mutants (Fig. 4e), CA-SMAD2 elicited a similar induction of *lft1* expression in *myo1g*-deficient animals

(Fig. 7c, Cohen's *d* effect size = 3.39 for MZ *myo1g* mutants versus 3.62 for WT controls).

The pharmacological Myosin antagonist Pentachloropseudilin (PCIP) inhibits TGF β signaling by regulating the membrane trafficking of TGF β type II receptors⁵³. In accordance with a potential function in membrane trafficking, Myo1G-GFP localizes to both the cell cortex and to intracellular, potentially endosomal, compartments (Fig. 7d). The endosomal protein SMAD Anchor for Receptor Activation (SARA) has been shown to promote the activation of the Nodal signal transducers SMAD2 and 3²⁹. We, therefore, investigated if Myo1G-GFP positive intracellular compartments correspond to SARA endosomes. Strikingly, the use of an established mRFP-SARA construct⁵⁴ revealed that in 24/24 embryos, SARA-positive compartments were always associated with Myo1G-GFP. Both standard laser scanning microscopy (Fig. 7e) and Airyscan super-resolution microscopy (Supplementary Fig. 12a, b) revealed that SARA-positive compartments are often part of larger, Myo1G-positive structures, in accordance with a potential role of Myo1G in the biology of TGF β signaling endosomes.

In murine lymphocytes, Myo1G regulates the endocytic trafficking of the adhesion protein CD44⁵⁵, a molecule that has, in other biological contexts, been shown to regulate TGF β signaling by acting as Hyaluronan receptor⁵⁶. In contrast to the situation described in the mouse immune system, our observations indicate that MZ *myo1g* mutants and WT controls have a similar number of CD44 endosomes (Fig. 7k, l and Supplementary Fig. 11b), suggesting thereby that Myo1G only regulates CD44 trafficking in specific biological contexts.

In the light of previous work linking MyosinI activity to TGF β type II receptor trafficking⁵³, we next investigated the importance of Myo1G for the trafficking of Activin type II receptors. The zebrafish genome harbors four *AcvrII* receptor genes (*acvrIIa*, *acvrIIb*, *acvrIIc*, *acvrIIe*). Our analysis revealed that *AcvrIIa*-GFP, *AcvrIIb*-GFP, and *AcvrIIc*-HA fusions all localize to the cell cortex and to intracellular compartments, similar to the localization pattern observed for Myo1G itself (Fig. 7d–i and Supplementary Fig. 11c). A completely different localization pattern was observed for *AcvrIIb*, with similar behavior observed using a GFP-fusion generated in the course of the present work or a previously reported *AcvrIIb*-HA⁵⁷ construct (Supplementary Fig. 11d, e).

To study the potential impact of Myo1G on Activin receptor trafficking, we took advantage of our *AcvrIIa*-GFP and *AcvrIIb*-GFP constructs to quantify the number of *AcvrII* endosomes in MZ *myo1g* mutant and WT sibling embryos. Co-injection of a Histone2B-RFP construct was used to ensure that *AcvrII* endosomes were counted in animals that received comparable amounts of injected material. A first set of quantifications was carried out in blastoderm cells at the germ ring stage (onset of gastrulation, 5.5 h post fertilization). In accordance with a potential role of Myo1G in regulating *AcvrII* trafficking, our experiments reveal that MZ *myo1g* mutants present a significantly reduced number of *AcvrIIa* and *AcvrIIb* endosomes (Fig. 7f–j).

The observations that MZ *myo1g* mutants present a reduced number of *AcvrII* endosomes (Fig. 7f–j) and that Myo1G is found on SARA-positive compartments (Fig. 7e and Supplementary Fig. 12a, b) raise the question of whether Myo1G may be required for the formation of *AcvrII*/SARA-positive endosomes. Accordingly, MZ *myo1g* mutants present a reduction in the absolute number of SARA/*AcvrIIa*-positive compartments and a higher fraction of *AcvrIIa* compartments that lack the signaling endosome marker SARA (Fig. 8a–d). While the absolute numbers of endosomes observed at the germ ring and 12 somites stage cannot be compared due to technical reasons (see methods), a significant reduction of *AcvrIIa*+SARA double-positive endosomes is observed in MZ *myo1g* mutants compared to WT controls both at the germ ring stage when early signaling by the Nodal ligands Cyclops and Squint regulates germ layer specification (Fig. 8a–c) and at the 12 somites stage (15 hpf) in the lateral plate mesoderm, when Spaw-mediated Nodal signaling controls LR asymmetry (Fig. 8d and Supplementary Fig. 12c, d).

Interestingly, our analysis suggests that MZ *myo1g* mutants present stage-specific defects in SARA endosome dynamics: While *myo1g* loss of function has no effect on the absolute number of SARA-positive endosomes in blastoderm cells at the germ ring stage (Fig. 8c), MZ *myo1g* mutants present a significant reduction in the number of SARA endosomes that are present in the 12 somites stage LPM (Fig. 8d). The observation that the specific decrease of SARA endosomes at later developmental timepoints is also observed if mRFP-SARA is injected alone without *AcvrIIa*-GFP (Supplementary Fig. 12e) suggests that this phenotype is directly caused by the loss of function of Myo1G rather than being an indirect consequence of impaired *AcvrIIa*-GFP trafficking.

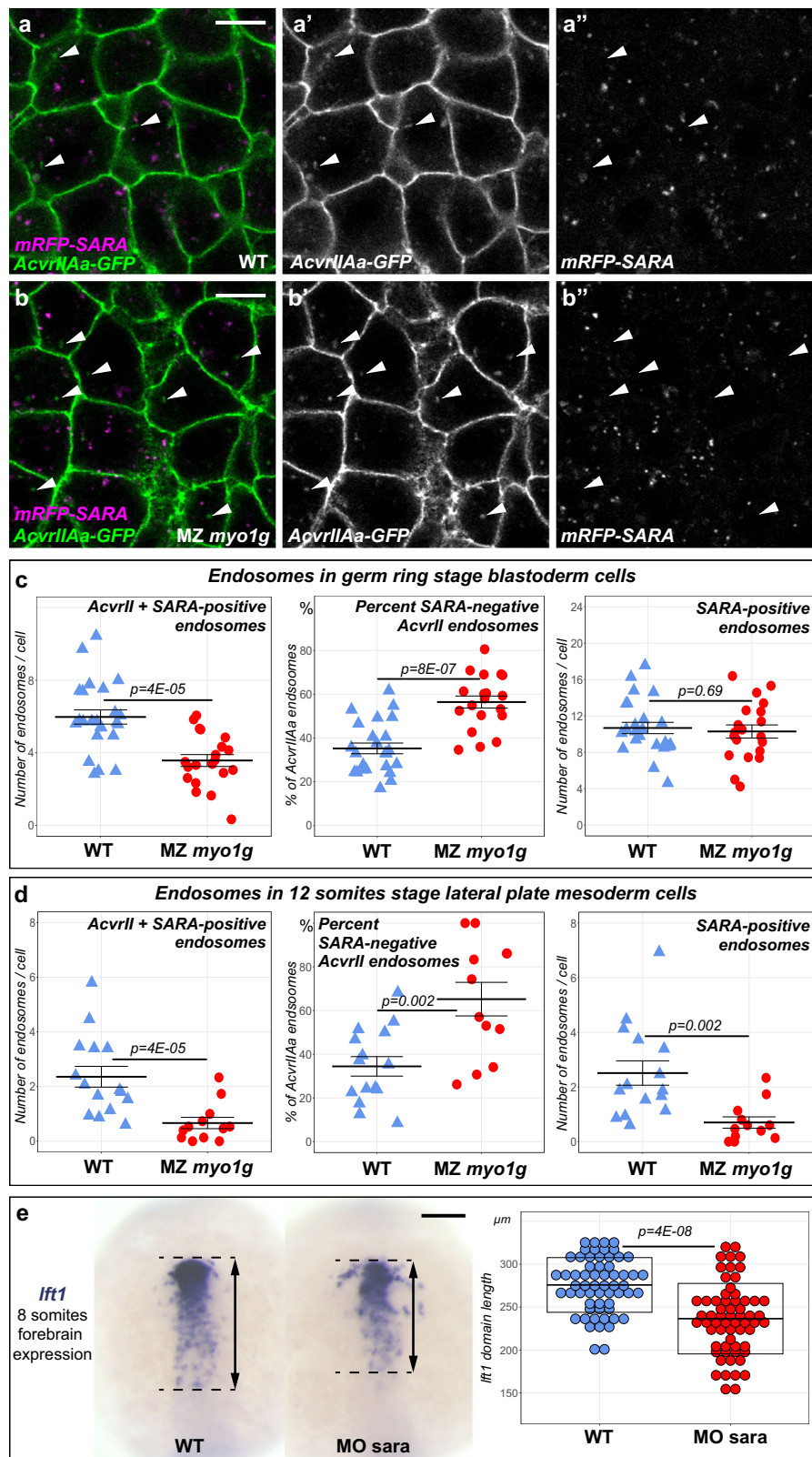
SARA contributes to context-dependent Nodal signaling. The observations that Myo1G is dispensable for early Nodal signaling during germ layer specification but required for later Nodal signaling in LR asymmetry and that *myo1g* loss of function causes a specific reduction in the number of SARA endosomes at later developmental stages raises the question of whether SARA may itself contribute to the regulation of Nodal signaling in specific developmental contexts. To address this question, we took advantage of a knock-down strategy that has been validated in previous work⁵⁴ in which both maternal and zygotic SARA functions are inhibited through the co-injection of one translation-blocking and one splice-blocking anti-sense morpholino oligonucleotide.

In accordance with previously reported phenotypes⁵⁴ and similar to MZ *myo1g* mutants, SARA morphant embryos failed to display morphological defects indicative of an impairment in Nodal-dependent germ layer specification. Specific examination of LR asymmetry revealed, however, partial but significant defects in cardiac jogging (Supplementary Fig. 13a). While cardiac jogging is impaired in MZ *myo1g* mutants and SARA morphants, it is important to note that the jogging defects that are observed in the two types of animals are distinct: SARA morphants present a predominant occurrence of right-ward cardiac jogging (Supplementary Fig. 13a) while the defect most frequently observed in MZ *myo1g* mutants is a lack of jogging that leaves the heart in the middle (Fig. 1a). The occurrence of distinct laterality phenotypes was confirmed through the examination of *spaw* expression in the lateral plate mesoderm, with a reduction in left-sided *spaw* expression predominating in MZ *myo1g* mutants (Supplementary Fig. 3a) while SARA morphants frequently display bilateral *spaw* expression (Supplementary Fig. 13b).

Bilateral *spaw* expression can be indicative of defects in the formation of a functional midline barrier that restrains Spaw propagation^{32,33}. To investigate the status of midline structures in SARA morphants, we performed *in situ* hybridizations against *foxa1* which is normally expressed in midline cells of the floorplate and hypochord (located respectively above and below the notochord). SARA morphants present discontinuities in the hypochord (red arrowheads in Supplementary Fig. 13d) as well ectopic *foxa1* expression in the notochord (green arrowheads in Supplementary Fig. 13d) that is normally devoid of staining (Supplementary Fig. 13c), indicating a defect in midline cell fate specification.

Although SARA was initially identified as a TGF β signaling adapter²⁹, subsequent studies revealed an additional function of SARA in promoting Notch signaling during spinal cord development⁵⁴. As Notch signaling is also required for the specification of midline cell fates (including hypochord development)^{58,59} we investigated the status of Notch signaling in SARA morphants and observed a marked downregulation of the Notch target genes *her4.1* and *her15.1* (Supplementary Fig. 13e–h).

Our observations suggest, therefore, that, through its function in Notch signaling⁵⁴, SARA contributes to the establishment of a functional midline barrier. As the midline barrier acts as a natural brake for



Nodal signaling, the midline function of SARA prevented us from addressing its specific contribution to MyoIG-dependent Spaw signaling. While the observations that SARA morpholino injection enhances the defects of MZ *myo1g* mutants that are observed with respect to cardiac jogging (Supplementary Fig. 13i) and *spaw* expression (Supplementary Fig. 13j) are in potential accordance with a contribution of SARA to MyoIG/Spaw signaling, establishing such a

function unambiguously would require to specifically inhibit only Notch-independent SARA activities.

To circumvent this problem, we analyzed the effect of SARA loss of function on the forebrain expression of *ift1*, which occurs in response to MyoIG-dependent Nodal signaling (Fig. 6c) and is independent of the more posteriorly located midline barrier. Similarly to MZ *myo1g* mutants, SARA morphants present a significantly reduced

Fig. 8 | MZ *myo1g* mutants present stage-specific endosomal trafficking defects. **a, b** MZ *myo1g* mutants present an increased number of SARA-negative AcvrIIAa endosomes (white arrowheads). Animal pole views of germ ring stage blastoderm cells. Scale bars: 10 μm . **c, d** Quantifications of AcvrIIAa/SARA-positive endosomes in WT control and MZ *myo1g* mutant cells in the germ ring stage blastoderm (**c**) and the 12 somites stage Lateral Plate Mesoderm (**d**, see also Supplementary Fig. 12c, d). Left panels: Mean number of AcvrIIAa-GFP and mRFP-SARA double-positive endosomes per cell. Middle panels: Percentage of the total number of AcvrIIAa endosomes per cell that are SARA-negative. Right panels: Number of SARA endosomes per cell. The absolute number of AcvrIIAa+SARA double-positive endosomes decreases and the fraction of SARA-negative AcvrIIAa endosomes increases both in

the early blastoderm (**c**) and later lateral plate mesoderm (**d**). In contrast, the mean number of SARA endosomes per cell remains unchanged in MZ *myo1g* mutants at the early germ ring stage while being significantly decreased at 12 somites. In **c, d** data points represent the mean number of endosomes per cell for a particular embryo and lines indicate the overall mean \pm SEM. **e** Eight-somites stage SARA morphants (MO sara) present a reduction in the antero-posterior extension of forebrain *lft1* expression. Dorsal views of the brain, anterior up. Scale bar: 100 μm . Box plots in **e** indicate mean values \pm SD. All *p* values were obtained using non-directional statistical tests. Complete numerical and statistical information for all experiments are provided in the Source Data files.

antero-posterior extension of the *lft1* expression domain (Fig. 8e). Taken together, our findings suggest that SARA acts, like Myo1G, to promote Nodal signaling in specific biological contexts.

Discussion

A striking feature of LR asymmetry is that different species use seemingly distinct mechanisms for the determination of this body axis³. Only recently has the unconventional type I Myosin Myo1D, which was initially identified as a regulator of *Drosophila* laterality^{34,35}, been identified as an evolutionarily conserved regulator of animal LR asymmetry⁴⁻⁷. While studies in fish and frogs uncovered an essential role of Myo1D in LRO morphogenesis⁴⁻⁶, several observations suggest that additional functions of Myosin1 proteins in LR asymmetry remain to be uncovered. First, previous studies had identified a function of Myo1D in the central LRO of fish and frogs, a biological structure that has no equivalent in *Drosophila*, where Myo1D ensures a local, organ-specific control of chiral morphogenesis. Second, in contrast to the unique *myo1d* gene present in flies, vertebrate genomes harbor not only *myo1d*, but also the closely related *myo1g*. We present an analysis of the function of this second *myosin1* homolog in zebrafish and uncover an essential function of this gene in chiral morphogenesis that is distinct from the one exerted by *myo1d*⁴⁻⁶.

Myo1D controls the symmetry-breaking ciliary fluid flow in the central LRO⁴⁻⁶. Accordingly, *myo1d* loss of function causes defects in all lateralized organs⁴⁻⁶. In contrast, *myo1g* is required for the chiral morphogenesis of the heart and brain, but dispensable for visceral laterality (Fig. 1 and Supplementary Fig. 2). To specifically determine if Myo1G exerts an LRO flow-independent function, we inactivated *myo1g* in the context of animals that lack the ciliary motility gene *dnaaf1* and therefore have no LRO flow. Lack of a LRO flow in *dnaaf1* mutants causes a distinctive randomization of LR asymmetry, in which the heart, brain, and viscera develop either normally or as their mirror image. In contrast, a different phenotype is observed in *dnaaf1* MZ *myo1g* double (or *dnaaf1* MZ *myo1d* MZ *myo1g* triple) mutants where cardiac and brain laterality are altogether lost (Fig. 1). These findings establish an essential role of Myo1G in the flow-independent, tissue-specific control of LR asymmetry.

How does Myo1G exert this tissue-specific control? Myo1G could be involved in the local, organ-specific execution of chiral morphogenesis, like *Drosophila myo1d*^{48,35}. Alternatively, Myo1G could be involved in the transmission of laterality information from the central LRO to different target tissues. While our experiments do not rule out the first possibility, MZ *myo1g* mutants present a reduced propagation of the Nodal ligand *spaw* and a reduction in the expression of different Nodal target genes (Fig. 2 and Supplementary Fig. 3). Our observations that residual *spaw* expression still reaches the posterior visceral primordium in MZ *myo1g* mutants (Supplementary Fig. 6), but fails to reach the more anterior cardiac territory (Fig. 3c, c' and Supplementary Fig. 5) provides a potential explanation for the tissue-specificity of the observed laterality phenotypes. It is noteworthy that similar organ-specific laterality phenotypes are observed in zebrafish *furin* mutants that present a reduced Nodal signaling range due to impaired Nodal proprotein maturation⁴³.

The conclusion that Myo1G is important for the Spaw-mediated control of LR asymmetry is further supported by the observation of similar cardiac laterality defects in MZ *spaw* single and MZ *spaw* MZ *myo1g* double mutants (Supplementary Fig. 4c). The observation that MZ *myo1g* mutants can be rescued through Spaw or FurinA overexpression (Fig. 2e, f) shows that Nodal signaling is reduced but not abolished in these animals. Quantitative analysis of Spaw-dependent gene induction indeed reveals that the responsiveness to Nodal ligands is reduced in MZ *myo1g* mutant embryos (Fig. 4).

In addition to the specific function of Spaw in LR asymmetry, two other zebrafish Nodal ligands, *Cyc* and *Sqt* play major roles in germ layer specification and patterning^{40,47,48}. Although MZ *myo1g* mutants show a reduced response to ectopic *Cyc/Sqt* expression (Fig. 5a, b), they do not display phenotypes indicative of defects in *Cyc/Sqt*-dependent germ layer specification (Fig. 5f). MZ *myo1g* mutants do however display a reduced expression of Nodal target genes in different biological contexts at later developmental stages. Importantly a number of defects are observed well before the onset of *spaw* expression, e.g. in the tail bud region by the end of gastrulation (Fig. 6a, b), or in tissues that do not express *spaw* altogether (8 somites stage forebrain, Fig. 6c) demonstrating thereby that Myo1G is important for the context-dependent regulation of signaling by different Nodal ligands.

How does Myo1G control Nodal signaling? Myo1G localizes to the cellular cortex and to intracellular compartments that our experiments show to be positive for the endosomal TGF β signaling adapter SARA²⁹ (Fig. 7d, e), suggesting thereby that Myo1G may regulate the endosomal trafficking of Nodal pathway components. In accordance with this hypothesis, MZ *myo1g* mutants present a reduction in the number of endosomes that are positive for both SARA and Activin type II receptor (AcvrII) molecules (Figs. 7, 8).

How could the interplay between Myo1G, SARA, and AcvrII exert a context-specific regulation of Nodal signaling? While we cannot provide a definitive answer to this question at the present moment, we envisage two major hypotheses: On one hand, early and late nodal signaling may require different receptor complexes. Genetic studies of zebrafish AcvrII function have indeed revealed that AcvrII receptors are dispensable for early Nodal signaling in germ layer specification⁶⁰, a finding that is in perfect accordance with our observation that Myo1G, which controls AcvrII trafficking, is itself not important for early *Cyc/Sqt* signaling. An alternative explanation for the occurrence of late but not early Nodal signaling phenotypes in MZ *myo1g* mutants could be that Nodal-related membrane trafficking and signaling are regulated differently according to the biological context. Our observation that MZ *myo1g* mutants present a reduction in the number of SARA endosomes in the 12 somites stage LPM but not in the germ ring stage blastoderm (Fig. 8c, d and Supplementary Fig. 12e) does indeed point to this direction. Interestingly, SARA and Myo1G are both dispensable for Nodal-dependent early germ layer specification (ref. 54 and Fig. 5f) but required to promote the expression of the nodal target gene *lft1* during later forebrain development (Figs. 6c, 8e).

Taken together, our findings identify Myo1G as a context-dependent regulator of Nodal signaling whose function is specifically

required for LR asymmetry. Investigating the molecular mechanism that underlies this context-dependent regulation will be an interesting aim for future studies. Finally, our work establishes a link between unconventional type I Myosins that are emerging as major regulators of animal laterality, and Nodal signaling, which has long been known to be the key pathway regulating vertebrate LR asymmetry.

Methods

Use of research animals

Zebrafish experiments have been performed in accordance with animal welfare guidelines in the iBV zebrafish facility (authorization #C06-088-17) in the context of the authorized animal experimentation projects APAFIS#5521-201605111041958v6 and APAFIS#15157-201805012112438v2, approved by the animal experimentation ethical committee Ciepál Azur.

Zebrafish strains and embryo maintenance

Embryos were raised in 0.3X Danieau medium (17.4 mM NaCl, 0.21 mM KCl, 0.12 mM MgSO₄, 0.18 mM Ca (NO₃)₂, 1.5 mM Hepes, pH 7.6) at 28.5 °C and staged according to standard criteria⁶¹. If necessary, 1-phenyl-2-thiourea (Sigma) was added at 30 mg/l to prevent embryonic pigmentation.

myo1d inactivations were performed using the previously reported *myo1d*^{tj16b} or *myo1d*^{tj16c} alleles⁵. With the exception of Fig. 2b, *myo1g* inactivations were performed using the previously reported *myo1g*^{tj18c} allele⁵. The analysis of *spaw* expression in the LLPM (Fig. 2b) additionally includes animals carrying the *myo1g*^{tj18c} and *myo1g*^{tj18e} alleles described below. Details concerning the mutant alleles used in different experiments are in the Source data files. All presented data were obtained using Maternal Zygotic (MZ) MZ *myo1d* or MZ *myo1g* single or MZ *myo1d* MZ *myo1g* double mutants.

Allele-specific PCR was used to identify the WT *myo1d* allele (forward primer 5'-AGAGTGGAGCTGGAAAAACAGA-3', reverse primer 5'-CCCATCCCTCGTGAATAACTAAATCAC-3', 339 bp amplicon) as well as the mutant alleles tj16b (forward primer 5'-TGGAGCTGGAAAA GGCTCGT-3', reverse primer 5'-CCATCACTGCAGCAGAAATGAGAG-3', 133 bp amplicon) and tj16c (forward primer 5'-GTGGAGCTGGAAA AAGGCTATAC-3', reverse primer 5'-CCATCACTGCAGCAGAAATGA GAG-3', 145 bp amplicon).

The allele-specific reverse primers 5'-TCTCATACAGTTCTCT TCCCCTAG-3' (tj18b, 115 bp amplicon), 5'-GAGGTGGATTCTCATA CAGTTCTCTTCTCAA-3' (tj18c, 120 bp amplicon), 5'-TCTTCCCTCG GATGCTTCC-3' (tj18e, 115 bp amplicon) and 5'- CTCATACAGTTCT CTCCCCTGTAG-3' (WT, 120 bp amplicon) were used with the generic forward primer 5'-GAGAAGAGTCGTATCTACACCTTC-3' to genotype *myo1g* mutant fish. The *myo1g*^{tj18c} and *myo1g*^{tj18e} alleles both cause frame shift mutations after amino acid 64 due to a 10 bp deletion (CTACAGGGGA, *myo1g*^{tj18c}) or a 6 bp deletion/13 bp insertion (CTA CAG => GGAAGACATCCGA, *myo1g*^{tj18e}) in the *myo1g* open reading frame.

myo1Cb inactivation was performed using the *myo1Cb*^{sa16637} allele from the Zebrafish Mutation Project (<http://www.sanger.ac.uk/resources/zebrafish/zmp/>) obtained from the Zebrafish International Resource Center. The *sa16637* allele introduces a premature stop codon at the 228th amino acid position. A generic forward primer 5'-GTCACATCCTGAACCTGCTAG-3' was used along with a mutant-specific reverse primer 5'-TATTACCAGTATCTGGTCAAG-3' (164 bp amplicon) to identify the mutant allele. The WT allele was identified using the generic forward primer with the WT-specific reverse primer 5'- CAGTACCAGTATCTGGTCAAG-3' (164 bp amplicon).

dnaaf1 was inactivated using the *dnaaf1*^{tm317b} mutant allele⁴¹. The forward primer 5'- GCAAGCTTTGCACGCTTAATGTCTC -3' and reverse primer 5'- AACACTGGAGAAATGTTTGAC - 3' were used to amplify the tm317b mutant allele (199 bp amplicon). The *dnaaf1* WT allele was identified using the forward primer 5'-GCAAGCTTTGCA

CGCTTAATGTCTC-3' and reverse primer 5'-CACACTGGAGAATGTT TGTGAC-3' (199 bp amplicon). Beyond 24 h of development, *dnaaf1* mutants can be identified through the oval phenotype that is diagnostic for ciliary mutations.

spaw was inactivated using the *spaw*^{s457} allele⁶². The alternative forward primers 5'-AACCTCTCCATTCGCAAA-3' (recognizing the s457 allele) 5'-AACCTCTCCATTCGCAAT-3' (recognizing the WT allele) were used together with the generic reverse primer 5'-GGATAAACTGG CTGGAG-3' to yield 156 bp amplicons.

Plasmid generation

The *myo1g* ORF was amplified from a mixed stage pool of cDNAs using primers 5'-GATCCCATCGATTTCGATGGCGGAGCTGGAGGGCTTG-3' and 5'-AGGCTCGAGAGGCCTTACTGGGCGAGGTAAGG-3' and cloned into the pCS2+ vector using Gibson assembly mix (NEB). Bold letters in the primer sequences indicate Gibson overhangs that are also present in the pCS2+ sequence. For generating the *myo1g*-GFP construct, the *myo1g* ORF was amplified from the *myo1g*-pCS2 construct using the primer pair

5'-GCAGATCCCATCGATTTCGACAGTAAACATGGCGGAGCTGG AGGGCTTG-3' and

5'-ACCATGGACCCTCCGCTGGTGCCTGGGCGAGGAGTAAGGTA AATC-3', and was ligated onto GFP-pCS2 +. *CD44a* was amplified using the primers 5'-ATCCCATCGATTTCGACAGTAAACATGTGGACTTTGTT ATTTGTAGTGT-3' and 5'- ACCATGGACCCTCCGCTGGTGCCTTAA AATATTCTTTTTCTGTTCA-3' and ligated into GFP-pCS2+. For the cloning of different AcvrII-GFP constructs, the following primers were used: AcvrIIAa 5'-GGATCCCATCGATTTCGACAGTAAACATGGGACCT GCAACAAAGCTGGC-3' (forward) and

5'-ACCATGGACCCTCCGCTGGTGCCTAGACTAGACTCCTTTGGGG GATA-3' (reverse), AcvrIIAb 5'-GGATCCCATCGATTTCGACAGTAA ACATGGTCAAGCGGGCTGTGGCT-3' (forward) and 5'-TCACCATGG ACCCTCCGCTGGTGCCTAGGCTGGACTCTTTAGGCGGA-3' (reverse), AcvrIIBa 5'- GATCCCATCGATTTCGACAGTAAACATGTTCGTTCTCTGC TCACTTTGG-3' (forward) and 5'-ACCATGGACCCTCCGCTGGTGC C-GATGCTGGACTCTTTGGGCGG-3' (reverse) to amplify the ORFs, which were ligated into GFP-pCS2+. The *her4.1*-pBSK construct used to generate an in situ probe was cloned using the primer pair 5'- GT CGACGGTATCGATAAGCCACACAGCAATGACTCCTAC-3' and

5'-CTAGAAGTGGATCCCCCTTAAGTCTACCAGGGTCTCC-3'. *her15.1* was amplified using the forward primer 5'-GTCGACGGTATC GATAAGCGCTCAGAGAAACAGCATCTCTCC-3' and reverse primer 5'-CTAGAAGTGGATCCCCCTCCACAGGAGTTCACATTG AC-3' and cloned into pBSK.

RNA and morpholino injections

mRNAs were synthesized using the SP6 mMessage mMachine kit (Ambion). RNAs were diluted in 0.1M KCl 0.2% Phenol Red. The following constructs and quantities were used: AcvrIIAa-GFP-pCS2+ (12.5/25 pg, this study), AcvrIIAb-GFP-pCS2+ (25 pg, this study), AcvrIIAb-HA-pCS2+ (25 pg⁵⁷), AcvrIIBa-GFP-pCS2+ (12.5/25 pg, this study), AcvrIIBb-HA-pCS2+ (25 pg⁵⁷), CA-SMAD2-pCS2+ (20 pg⁶³), CD44a-GFP-pCS2+ (50 pg, this study), GFP-Spaw-pCS2+ (20 pg⁴³), FurinA-pCS2+ (2.5 pg⁴³), Histone2B-mRFP-pCS2+ (12.5 pg⁶⁴), mRFP-SARA-pCS2+ (12.5/25 pg⁵⁴), Myo1G-pCS2+ (50 pg, this study), Myo1G-GFP-pCS2+ (50 pg, this study). For Spaw⁶⁵, Cyclops⁶⁶, and Squint³⁹, different concentrations used in individual experiments are indicated in the figures. For technical reasons, AcvrIIAa-GFP and mRFP-SARA were injected at 25 pg each for the analysis of Acvr/SARA endosomes at germ ring stages (Fig. 8c), while injection was carried out at 12.5 pg each for analysis in the 12 somites stage lateral plate mesoderm (Fig. 8d). Different concentrations were used at the two developmental stages to warrant sufficient labeling for imaging while at the same time preventing the occurrence of overexpression phenotypes. No attention should, therefore, be paid to the difference in

the absolute number of endosomes that are observed at the two developmental stages.

The previously reported *dnaaf1* Morpholino 5'-ATGCACTG-TAATTTACCAAGTCAGG-3'³⁶ was injected at a concentration of 500 μ M. SARA knock-down was accomplished using a previously established combination⁵⁴ of a translation-blocking morpholino (5'-CA TGAAACTCCACCTGCCAAGCGT-3') and a splice-blocking morpholino (5'-TGAAGTAGAGACTTTACCTTGCCAC-3') injected at 150 μ M each. *cyclops* (5'-GCGACTCCGAGCGTGTGCATGATG-3') and *squint* (5'-ATGTCAAATCAAGGTAATAATCCAC-3') were inhibited using previously validated morpholinos⁶⁷. *cyc* and *sqt* morpholinos were injected either separately (*cyc* 64 μ M, *sqt* 250 μ M) or in combination (*cyc* 8 μ M, *sqt* 31 μ M). All morpholinos were diluted in 1x Danieau 0.2% Phenol Red.

For rescuing the cardiac jogging defects of *myo1g* mutant by Spaw mRNA injection, a mix of untagged Spaw RNA and GFP RNA was co-injected into one blastomere of two-cell stage embryos. At bud stage, embryos with a unilateral segregation of GFP expressing cells were selected using a fluorescent dissection scope (Leica M205FA), and grown further to score for cardiac jogging and looping phenotypes.

RNA in situ hybridization

Whole mount RNA in situ hybridizations were performed as previously described⁶⁸. For the following genes probes were transcribed from previously reported plasmids: *flh*-pBSK⁶⁹, *spaw*-pGEMT⁶⁵, *lefty1*-pBSK³¹, *lefty2*-pBSK³³, *otx5*-pBSK⁷⁰, *pitx2c*-pBSK⁷¹, *foxa1*-pBSK⁷², *cyclops*-pBSK³⁹, *dand5*-pBSK²⁴, *sox32*-pBSK⁷³, *sox17*-pBSK⁷⁴, *odad1*-pME18S-FL3⁶⁸, *dnah9*-pCR11⁷⁵, *foxl1a*-pBSK⁷⁶, *cmlc2*/*myl7*-pCS2⁷⁷, *gdf3*-pBSK⁶⁸, *Her4.1*-pBSK (this study), *Her15.1*-pBSK (this study). The *elovl6* probe was transcribed from a PCR product containing a T7 promoter sequence at the 3' end. *elovl6* was amplified from genomic DNA using the forward primer 5'-CCCGTCCCATGTGCAGAACATTG-3' and the reverse primer 5'-GGTGTCCATTGTGCTCGTGTCTCCCTATAGTAGTCGTATTACGC-3'.

qPCR analysis

qPCR was performed using PowerUP SYBR Green Master Mix (Applied Biosystems) in an Applied Biosystems Step-One PCR system. Individual reactions were performed in triplicates to account for pipetting errors. For sample preparation, whole cell mRNA was isolated from 50 embryos using TRI-Reagent (Sigma). Reverse transcription was performed from 2.5 μ g of RNA using Superscript III (Invitrogen) to generate cDNA. Fold changes in gene expression were normalized to the internal control gene *36b4*. The primers used for the amplification reactions are as follows: *lefty1*: forward 5'-AGAGGAGTTTGGGTCTAGTGG-3', reverse 5'-TACGGAGAGAGGAAATGCG-3'. *Spaw*: forward 5'-TGAC TTCGTCCTGAGCTTGA-3', reverse 5'-TCAAGCTCAGGACGAAGTCA-3'. *36b4*: forward 5'-ACGTGGAAGTCCAAGTACT-3', reverse: 5'-GTCA-GATCCTCCTGGTGA-3'. For estimating relative gene expression, the Ct values at 40 cycles of qPCR amplification were used according to the $\Delta\Delta$ CT method⁷⁸. Individual data points in figures documenting qPCR experiments correspond to technical replicates. Complete statistical information, including numbers of biological and technical replicates, is provided in the Source Data files.

Immunocytochemistry

For Acvr11-HA antibody stainings, dechorionated embryos were fixed for 1.5 h at Room temperature in PEM (80 mM Sodium-Pipes, 5 mM EGTA, 1 mM MgCl₂) - 4% PFA - 0.04% TritonX100 and then washed 2 \times 5 min in PEMT (PEM - 0.2% TritonX100), 10 min in PEM 50 mM NH₄Cl, 2 \times 5 min in PEMT. Before incubation with primary antibody (Rat@HA, Roche 11867423001, used at 1:1000), embryos were blocked for a minimum of 2 h through preincubation in PEMT + 5% normal goat serum. Following primary antibody incubation, embryos were washed

5 - 10 - 4 \times 15 min in PEMT before blocking again for a minimum of 2 h through preincubation in PEMT + 5% NGS, before incubation with the secondary antibody (Goat@Rat-Alexa488, Invitrogen A11006, used at 1:500). Following secondary antibody incubation, embryos were washed 5 - 10 - 4 \times 15 min in PEMT.

For Phospho-SMAD2/3 antibody stainings, dechorionated embryos were fixed overnight at 4 $^{\circ}$ C in PBS - 4% PFA and then dehydrated through 5 min washes in PBS-25/50/75% Methanol before being stored in Methanol at -20 $^{\circ}$ C for at least 12 h. For immunostaining, embryos were rehydrated through 5 min washes in 75/50/25% Methanol-PBS. Embryos were then washed 4 \times 5 min in PBS-1% Triton X-100, incubated 20 min in Acetone at -20 $^{\circ}$ C, and washed again 4 \times 5 min in PBS-1% Triton. Before incubation with primary antibody (Rabbit@Phospho-SMAD2/3, Cell Signaling 8828 S, used at 1:2000) embryos were blocked for a minimum of 2 h through preincubation in PBS-Triton + 10% fetal bovine serum. Following primary antibody incubation, embryos were washed 8 \times 15 min in PBS-Triton before blocking again for a minimum of 2 h through preincubation in PBS-Triton + 10% FBS, before incubation with the secondary antibody (Goat@Rabbit-AlexaFluorPlus488, Invitrogen A32731, used at 1:500). Following secondary antibody incubation, embryos were washed 8 \times 15 min in PBS-Triton.

Microscopy and image analysis

Imaging was performed using Laser scanning confocal microscopes (Zeiss LSM710, 780 and 880). Airyscan super-resolution imaging was performed on a Zeiss LSM 880 system. For confocal imaging of Phospho-SMAD2/3 antibody stainings, embryos were incubated in Mowiol, the yolk removed manually, and the embryos flat-mounted between slide and coverslip for confocal imaging using a 10x dry objective.

For all other experiments, embryos were mounted in 0.75% low melting agarose (Sigma) in glass bottom dishes (Mattek) for confocal imaging using a 40x NA 1.1 water immersion objective.

In situ hybridizations were documented on a Leica M205 microscope with a Lumenera Infinity camera.

Image analysis was performed using ImageJ (<http://rbs.info.nih.gov/ij/>).

For Spaw-GFP intensity measurements (Supplementary Fig. 11a), Spaw-GFP signals of individual embryos were measured relative to the intensity of the co-injected Histone2B-RFP construct to correct for differences in the amount of injected material received by each embryo. To allow comparison between WT and MZ *myo1g* mutants, the mean Spaw-GFP intensity signal of the WT control population was then set to 1 and data from all individual embryos normalized with respect to this value.

For *gdf3* LRO intensity measurements (Supplementary Fig. 10), RGB images were transformed to Luminance representations. Following the detection of the *gdf3* signal through automated thresholding, integrated density signals were measured in ROIs that comprise the LRO but exclude the non-LRO *gdf3* signal from the lateral mesoderm.

Statistical analyses

Appropriate statistical tests were selected for each experiment based on the nature of the comparison (bi- or multifactorial, ordinal or categorical data), data distribution, and variance. Statistical analysis and representations were performed using R/R-Studio. Complete information regarding the applied statistical tests, test statistics, sample sizes and displayed error bars for all experiments are provided in the Source Data files.

Reporting summary

Further information on research design is available in the Nature Portfolio Reporting Summary linked to this article.

Data availability

Source data are provided as Source Data files. Datasets and materials that were generated and analyzed during the current study are available from the corresponding author on request. Source data are provided with this paper.

References

- Hamada, H. Molecular and cellular basis of left-right asymmetry in vertebrates. *Proc. Jpn. Acad. Ser. B Phys. Biol. Sci.* **96**, 273–296 (2020).
- Schweickert, A. et al. Vertebrate left-right asymmetry: what can nodal cascade gene expression patterns tell us? *J. Cardiovasc. Dev. Dis.* **5**, 1 (2017).
- Hamada, H. & Tam, P. Diversity of left-right symmetry breaking strategy in animals. *F1000Res* **9**, F1000 (2020).
- Tingler, M. et al. A conserved role of the unconventional myosin 1d in laterality determination. *Curr. Biol.* **28**, 810–816.e813 (2018).
- Juan, T. et al. Myosin1D is an evolutionarily conserved regulator of animal left-right asymmetry. *Nat. Commun.* **9**, 1942 (2018).
- Saydmohammed, M. et al. Vertebrate myosin 1d regulates left-right organizer morphogenesis and laterality. *Nat. Commun.* **9**, 3381 (2018).
- Alsafwani, R. S. et al. Novel. *Front. Med.* **8**, 724826 (2021).
- Nonaka, S. et al. Randomization of left-right asymmetry due to loss of nodal cilia generating leftward flow of extraembryonic fluid in mice lacking KIF3B motor protein. *Cell* **95**, 829–837 (1998).
- Hashimoto, M. et al. Planar polarization of node cells determines the rotational axis of node cilia. *Nat. Cell Biol.* **12**, 170–176 (2010).
- Nonaka, S., Shiratori, H., Saijoh, Y. & Hamada, H. Determination of left-right patterning of the mouse embryo by artificial nodal flow. *Nature* **418**, 96–99 (2002).
- Kramer-Zucker, A. G. et al. Cilia-driven fluid flow in the zebrafish pronephros, brain and Kupffer's vesicle is required for normal organogenesis. *Development* **132**, 1907–1921 (2005).
- Essner, J. J. et al. Conserved function for embryonic nodal cilia. *Nature* **418**, 37–38 (2002).
- Gros, J., Feistel, K., Viebahn, C., Blum, M. & Tabin, C. J. Cell movements at Hensen's node establish left/right asymmetric gene expression in the chick. *Science* **324**, 941–944 (2009).
- Kajikawa, E. et al. Nodal paralogues underlie distinct mechanisms for visceral left-right asymmetry in reptiles and mammals. *Nat. Ecol. Evol.* **4**, 261–269 (2020).
- Levin, M., Thorlin, T., Robinson, K. R., Nogi, T. & Mercola, M. Asymmetries in H⁺/K⁺-ATPase and cell membrane potentials comprise a very early step in left-right patterning. *Cell* **111**, 77–89 (2002).
- Lebreton, G. et al. Molecular to organismal chirality is induced by the conserved myosin 1D. *Science* **362**, 949–952 (2018).
- Taniguchi, K. et al. Chirality in planar cell shape contributes to left-right asymmetric epithelial morphogenesis. *Science* **333**, 339–341 (2011).
- González-Morales, N. et al. The atypical cadherin dachsous controls left-right asymmetry in *Drosophila*. *Dev. Cell* **33**, 675–689 (2015).
- Naganathan, S. R., Fürthauer, S., Nishikawa, M., Jülicher, F. & Grill, S. W. Active torque generation by the actomyosin cell cortex drives left-right symmetry breaking. *Elife* **3**, e04165 (2014).
- Kuroda, R., Endo, B., Abe, M. & Shimizu, M. Chiral blastomere arrangement dictates zygotic left-right asymmetry pathway in snails. *Nature* **462**, 790–794 (2009).
- Minegishi, K. et al. A Wnt5 activity asymmetry and intercellular signaling via PCP proteins polarize node cells for left-right symmetry breaking. *Dev. Cell* **40**, 439–452.e434 (2017).
- Borovina, A., Superina, S., Voskas, D. & Ciruna, B. Vangl2 directs the posterior tilting and asymmetric localization of motile primary cilia. *Nat. Cell Biol.* **12**, 407–412 (2010).
- Hill, C. S. Establishment and interpretation of NODAL and BMP signaling gradients in early vertebrate development. *Curr. Top. Dev. Biol.* **149**, 311–340 (2022).
- Hashimoto, H. et al. The Cerberus/Dan-family protein Charon is a negative regulator of Nodal signaling during left-right patterning in zebrafish. *Development* **131**, 1741–1753 (2004).
- Sampaio, P. et al. Left-right organizer flow dynamics: how much cilia activity reliably yields laterality? *Dev. Cell* **29**, 716–728 (2014).
- Maerker, M. et al. Bicc1 and Dicer regulate left-right patterning through post-transcriptional control of the Nodal inhibitor Dand5. *Nat. Commun.* **12**, 5482 (2021).
- Minegishi, K. et al. Fluid flow-induced left-right asymmetric decay of Dand5 mRNA in the mouse embryo requires a Bicc1-Ccr4 RNA degradation complex. *Nat. Commun.* **12**, 4071 (2021).
- Gritsman, K. et al. The EGF-CFC protein one-eyed pinhead is essential for nodal signaling. *Cell* **97**, 121–132 (1999).
- Tsakazaki, T., Chiang, T. A., Davison, A. F., Attisano, L. & Wrana, J. L. SARA, a FYVE domain protein that recruits Smad2 to the TGFbeta receptor. *Cell* **95**, 779–791 (1998).
- Bodenstine, T. M., Chandler, G. S., Seftor, R. E., Seftor, E. A. & Hendrix, M. J. Plasticity underlies tumor progression: role of Nodal signaling. *Cancer Metastasis Rev.* **35**, 21–39 (2016).
- Thisse, C. & Thisse, B. Antivin, a novel and divergent member of the TGFbeta superfamily, negatively regulates mesoderm induction. *Development* **126**, 229–240 (1999).
- Lenhart, K. F., Lin, S. Y., Titus, T. A., Postlethwait, J. H. & Burdine, R. D. Two additional midline barriers function with midline lefty1 expression to maintain asymmetric Nodal signaling during left-right axis specification in zebrafish. *Development* **138**, 4405–4410 (2011).
- Bisgrove, B. W., Essner, J. J. & Yost, H. J. Regulation of midline development by antagonism of lefty and nodal signaling. *Development* **126**, 3253–3262 (1999).
- Hozumi, S. et al. An unconventional myosin in *Drosophila* reverses the default handedness in visceral organs. *Nature* **440**, 798–802 (2006).
- Spéder, P., Adám, G. & Noselli, S. Type ID unconventional myosin controls left-right asymmetry in *Drosophila*. *Nature* **440**, 803–807 (2006).
- Baker, K., Holtzman, N. G. & Burdine, R. D. Direct and indirect roles for Nodal signaling in two axis conversions during asymmetric morphogenesis of the zebrafish heart. *Proc. Natl Acad. Sci. USA* **105**, 13924–13929 (2008).
- Smith, K. A. et al. Rotation and asymmetric development of the zebrafish heart requires directed migration of cardiac progenitor cells. *Dev. Cell* **14**, 287–297 (2008).
- Rohr, S., Otten, C. & Abdelilah-Seyfried, S. Asymmetric involution of the myocardial field drives heart tube formation in zebrafish. *Circ. Res.* **102**, e12–e19 (2008).
- Rebagliati, M. R., Toyama, R., Fricke, C., Haffter, P. & Dawid, I. B. Zebrafish nodal-related genes are implicated in axial patterning and establishing left-right asymmetry. *Dev. Biol.* **199**, 261–272 (1998).
- Sampath, K. et al. Induction of the zebrafish ventral brain and floorplate requires cyclops/nodal signalling. *Nature* **395**, 185–189 (1998).
- Sullivan-Brown, J. et al. Zebrafish mutations affecting cilia motility share similar cystic phenotypes and suggest a mechanism of cyst formation that differs from pkd2 morphants. *Dev. Biol.* **314**, 261–275 (2008).
- Noël, E. S. et al. A Nodal-independent and tissue-intrinsic mechanism controls heart-looping chirality. *Nat. Commun.* **4**, 2754 (2013).

43. Tessadori, F. et al. Nodal signaling range is regulated by proprotein convertase-mediated maturation. *Dev. Cell* **32**, 631–639 (2015).
44. Petzoldt, A. G. et al. DE-cadherin regulates unconventional myosin ID and myosin IC in *Drosophila* left-right asymmetry establishment. *Development* **139**, 1874–1884 (2012).
45. Raya, A. et al. Notch activity induces Nodal expression and mediates the establishment of left-right asymmetry in vertebrate embryos. *Genes Dev.* **17**, 1213–1218 (2003).
46. Montague, T. G., Gagnon, J. A. & Schier, A. F. Conserved regulation of Nodal-mediated left-right patterning in zebrafish and mouse. *Development* **145**, dev171090 (2018).
47. Feldman, B. et al. Zebrafish organizer development and germ-layer formation require nodal-related signals. *Nature* **395**, 181–185 (1998).
48. Thisse, B., Wright, C. V. & Thisse, C. Activin- and Nodal-related factors control antero-posterior patterning of the zebrafish embryo. *Nature* **403**, 425–428 (2000).
49. Pelliccia, J. L., Jindal, G. A. & Burdine, R. D. Gdf3 is required for robust Nodal signaling during germ layer formation and left-right patterning. *Elife* **6**, e28635 (2017).
50. Perez-Hernandez, D. et al. The intracellular interactome of tetraspanin-enriched microdomains reveals their function as sorting machineries toward exosomes. *J. Biol. Chem.* **288**, 11649–11661 (2013).
51. McIntosh, B. B. & Ostap, E. M. Myosin-I molecular motors at a glance. *J. Cell Sci.* **129**, 2689–2695 (2016).
52. Arif, E. et al. The motor protein Myo1c regulates transforming growth factor- β -signaling and fibrosis in podocytes. *Kidney Int.* **96**, 139–158 (2019).
53. Chung, C. L. et al. Pentachloropseudilin inhibits transforming growth factor- β (TGF- β) activity by accelerating cell-surface type II TGF- β receptor turnover in target cells. *Chembiochem* **19**, 851–864 (2018).
54. Kressmann, S., Campos, C., Castanon, I., Fürthauer, M. & González-Gaitán, M. Directional Notch trafficking in Sara endosomes during asymmetric cell division in the spinal cord. *Nat. Cell Biol.* **17**, 333–339 (2015).
55. López-Ortega, O. & Santos-Argumedo, L. Myosin 1g contributes to CD44 adhesion protein and lipid rafts recycling and controls CD44 capping and cell migration in B lymphocytes. *Front. Immunol.* **8**, 1731 (2017).
56. Ito, T., Williams, J. D., Fraser, D. J. & Phillips, A. O. Hyaluronan regulates transforming growth factor- β 1 receptor compartmentalization. *J. Biol. Chem.* **279**, 25326–25332 (2004).
57. Fu, X. X. et al. A spatiotemporal barrier formed by Follistatin is required for left-right patterning. *Proc. Natl Acad. Sci. USA* **120**, e2219649120 (2023).
58. Appel, B. et al. Delta-mediated specification of midline cell fates in zebrafish embryos. *Curr. Biol.* **9**, 247–256 (1999).
59. Latimer, A. J., Dong, X., Markov, Y. & Appel, B. Delta-Notch signaling induces hypochord development in zebrafish. *Development* **129**, 2555–2563 (2002).
60. Preiß, H. et al. Regulation of Nodal signaling propagation by receptor interactions and positive feedback. *Elife* **11**, e66397 (2022).
61. Kimmel, C. B., Ballard, W. W., Kimmel, S. R., Ullmann, B. & Schilling, T. F. Stages of embryonic development of the zebrafish. *Dev. Dyn.* **203**, 253–310 (1995).
62. Kalogirou, S. et al. Intracardiac flow dynamics regulate atrio-ventricular valve morphogenesis. *Cardiovasc. Res.* **104**, 49–60 (2014).
63. Dick, A., Mayr, T., Bauer, H., Meier, A. & Hammerschmidt, M. Cloning and characterization of zebrafish smad2, smad3 and smad4. *Gene* **246**, 69–80 (2000).
64. Gong, Y., Mo, C. & Fraser, S. E. Planar cell polarity signalling controls cell division orientation during zebrafish gastrulation. *Nature* **430**, 689–693 (2004).
65. Long, S., Ahmad, N. & Rebagliati, M. The zebrafish nodal-related gene southpaw is required for visceral and diencephalic left-right asymmetry. *Development* **130**, 2303–2316 (2003).
66. Rebagliati, M. R., Toyama, R., Haffter, P. & Dawid, I. B. cyclops encodes a nodal-related factor involved in midline signaling. *Proc. Natl Acad. Sci. USA* **95**, 9932–9937 (1998).
67. Dubrulle, J. et al. Response to Nodal morphogen gradient is determined by the kinetics of target gene induction. *Elife* **4**, e05042 (2015).
68. Thisse, B. et al. Spatial and temporal expression of the zebrafish genome by large-scale in situ hybridization screening. *Methods Cell Biol.* **77**, 505–519 (2004).
69. Talbot, W. S. et al. A homeobox gene essential for zebrafish notochord development. *Nature* **378**, 150–157 (1995).
70. Gamse, J. T. et al. Otx5 regulates genes that show circadian expression in the zebrafish pineal complex. *Nat. Genet.* **30**, 117–121 (2002).
71. Faucourt, M., Houliston, E., Besnardeau, L., Kimelman, D. & Lepage, T. The pitx2 homeobox protein is required early for endoderm formation and nodal signaling. *Dev. Biol.* **229**, 287–306 (2001).
72. Odenthal, J. & Nüsslein-Volhard, C. fork head domain genes in zebrafish. *Genes Evol.* **208**, 245–258 (1998).
73. Alexander, J., Rothenberg, M., Henry, G. L. & Stainier, D. Y. casanova plays an early and essential role in endoderm formation in zebrafish. *Dev. Biol.* **215**, 343–357 (1999).
74. Alexander, J. & Stainier, D. Y. A molecular pathway leading to endoderm formation in zebrafish. *Curr. Biol.* **9**, 1147–1157 (1999).
75. Essner, J. J., Amack, J. D., Nyholm, M. K., Harris, E. B. & Yost, H. J. Kupffer's vesicle is a ciliated organ of asymmetry in the zebrafish embryo that initiates left-right development of the brain, heart and gut. *Development* **132**, 1247–1260 (2005).
76. Yu, X., Ng, C. P., Habacher, H. & Roy, S. Foxj1 transcription factors are master regulators of the motile ciliogenic program. *Nat. Genet.* **40**, 1445–1453 (2008).
77. Rottbauer, W. et al. Cardiac myosin light chain-2: a novel essential component of thick-myofilament assembly and contractility of the heart. *Circ. Res.* **99**, 323–331 (2006).
78. Livak, K. J. & Schmittgen, T. D. Analysis of relative gene expression data using real-time quantitative PCR and the 2(-delta delta C(T)) method. *Methods* **25**, 402–408 (2001).

Acknowledgements

This study was supported by the ARC project grants PJA20181208167 (M.F.), PJA2023090007156 (M.F.), the ANR DroZeMyo (ANR-17-CE13-0024-02) (M.F.), and a CSI grant from Université Côte d'Azur (M.F.). A.J.K. benefited from a fourth-year PhD fellowship from La Ligue Contre le Cancer. Confocal microscopy was performed with the help of the iBV PRISM imaging platform. We thank J.Bakkers, J.Batut, E.Cau, P.Dufourcq, M.Gonzalez-Gaitan, C.P.Heisenberg, T.Lepage, S.Lopes, M.Roussigné, C. & B.Thisse, J.Vermot & PF Xu for the sharing of reagents. We are grateful to S.Polès, R.Rebillard, G.Dupuy, C.Girardin, and F.Salmy for technical assistance and excellent fish care.

Author contributions

The genetic analysis of *myosin1* function in zebrafish Nodal signaling was performed by A.J.K. F.B. generated reagents used in the present study. M.F. designed the study, performed experiments, analyzed the data, and wrote the manuscript.

Competing interests

The authors declare no competing interests.

Additional information

Supplementary information The online version contains supplementary material available at <https://doi.org/10.1038/s41467-024-50868-y>.

Correspondence and requests for materials should be addressed to Maximilian Fürthauer.

Peer review information *Nature Communications* thanks the anonymous reviewers for their contribution to the peer review of this work. A peer review file is available.

Reprints and permissions information is available at <http://www.nature.com/reprints>

Publisher's note Springer Nature remains neutral with regard to jurisdictional claims in published maps and institutional affiliations.

Open Access This article is licensed under a Creative Commons Attribution-NonCommercial-NoDerivatives 4.0 International License, which permits any non-commercial use, sharing, distribution and reproduction in any medium or format, as long as you give appropriate credit to the original author(s) and the source, provide a link to the Creative Commons licence, and indicate if you modified the licensed material. You do not have permission under this licence to share adapted material derived from this article or parts of it. The images or other third party material in this article are included in the article's Creative Commons licence, unless indicated otherwise in a credit line to the material. If material is not included in the article's Creative Commons licence and your intended use is not permitted by statutory regulation or exceeds the permitted use, you will need to obtain permission directly from the copyright holder. To view a copy of this licence, visit <http://creativecommons.org/licenses/by-nc-nd/4.0/>.

© The Author(s) 2024